RSC Advances

PAPER

View Article Online
View Journal | View Issue

Cite this: *RSC Adv.*, 2026, **16**, 2996

Design, synthesis, and biological evaluation of novel chalcone derivatives: integrating molecular docking with *in vivo* anti-inflammatory and antinociceptive studies

Abida Shamim,[a] Humaira Nadeem,[b] Syed Muzzammil Masaud,[b] Tajamul Hussain,[c] Kashif Bashir,[a] Salman Alrokayan,[d] Ihsan-ul Haq,[a] Muhamamd Latif,[efg] Muhammad Imran[h] and Nadeem Irshad *[a]

Chronic inflammatory disorders are often accompanied by persistent pain, yet current therapies remain limited by modest efficacy and adverse effects. To address this challenge, a series of eleven chalcone-based derivatives was synthesized *via* Claisen–Schmidt condensation and structurally characterized by FTIR, ^{1}H-NMR, ^{13}C-NMR, and EIMS analyses. Cytotoxicity assessment on 3T3 fibroblasts using the MTT assay revealed no toxicity compared to doxorubicin, while brine shrimp lethality and hemolytic assays further confirmed their safety profile. *In vitro* COX-1/2 assays demonstrated preferential inhibition of COX-2, with **AS1-6** showing a superior selectivity index relative to nimesulide. *In vivo* screening corroborated these results: **AS1-2**, **AS1-6**, and **AS1-8** produced significant anti-inflammatory effects in carrageenan-induced paw edema, while **AS1-2**, **AS1-6**, and **AS1-10** suppressed nociceptive behaviours in the formalin test, indicating both peripheral and central antinociceptive activity. *Ex vivo* ELISA further verified down-regulation of COX-2-associated inflammatory mediators compared to negative group. Molecular docking revealed strong and selective interactions of **AS1-2** and **AS1-6** within the COX-2 active site, while sparing COX-1. Molecular dynamics simulations confirmed the stability of **AS1-6** in the active pocket throughout a 100 ns trajectory, consistent with the pharmacological outcomes. Collectively, the concordance of *in vitro* COX-1/2 inhibition, *in vivo* efficacy, and *in silico* analyses underscores the potential of these chalcone analogues as selective COX-2 inhibitors. These findings highlight the value of structure-guided design in developing dual-function chalcones with anti-inflammatory and antinociceptive activity, warranting further optimization and preclinical evaluation.

Received 23rd September 2025
Accepted 22nd December 2025

DOI: 10.1039/d5ra07230a

rsc.li/rsc-advances

1 Introduction

Chalcones are α,β-unsaturated ketones characterized by a distinctive molecular structure that is integral to both synthetic chemistry and natural product synthesis. Their formation through Claisen–Schmidt condensation renders them highly versatile intermediates. Extensive research has shown that chalcones and their derivatives provide a vast range of biological activities, including anticancer properties, antioxidant, antihypertensive, anti-inflammatory, analgesic, antidiabetic, and antibacterial.[1] Natural chalcones remain of great interest due to their antioxidant and enzyme-modulating qualities, which offer mechanistic insights for creating better derivatives, in addition to their synthetic counterparts.[2] Due to their high solubility, chalcones are widely used as intermediates in organic reactions and the synthesis of flavonoids and isoflavonoids.[3] Prominent chalcone-based medications that have been authorized for clinical use include hesperidin, metochalcone, methyl chalcone, and sofalcone.[4] Compounds containing an acetamide derivatives

[a]*Department of Pharmacy, Faculty of Biological Sciences, Quaid-i-Azam University, Islamabad 45320, Pakistan. E-mail: abidashamim@bs.qau.edu.pk; kbashir@qau.edu.pk; ihaq@qau.edu.pk; nirshad@qau.edu.pk; Tel: +925190644099*

[b]*Riphah Institute of Pharmaceutical Sciences, Riphah International University, Islamabad, Pakistan. E-mail: humaira.nadeem@riphah.edu.pk; muzzammil.masaud@riphah.edu.pk*

[c]*Center of Excellence in Biotechnology Research, King Saud University, Riyadh 11451, Saudi Arabia. E-mail: thussain@ksu.edu.sa*

[d]*Research Chair for Biomedical Application of Nanomaterials, Biochemistry Department, College Fof Science, King Saud University, Riyadh 11451, Saudi Arabia. E-mail: salrokayan@ksu.edu.sa*

[e]*Centre for Genetics and Inherited Diseases (CGID), Taibah University, Madinah 42353, Saudi Arabia. E-mail: latifmayo@gmail.com*

[f]*Department of Basic Medical Sciences, College of Medicine, Taibah University, Madinah 42353, Saudi Arabia. E-mail: latifmayo@gmail.com*

[g]*Department of Chemistry, Rawalpindi Women University, Rawalpindi-46300, Pakistan. E-mail: latifmayo@gmail.com*

[h]*State Key Laboratory of Microbial Metabolism, Joint International Research Laboratory of Metabolic and Developmental Sciences, School of Life Sciences and Biotechnology, Shanghai Jiao Tong University, Shanghai, P. R. China. E-mail: imran93@sjtu.edu.cn*

have received much interest due to their varied medicinal activities, such as antioxidant, anticancer, analgesic, antimicrobial, and anti-inflammatory activities.[5] Acetamide derivatives, such as paracetamol, are known for their analgesic properties. Similarly, the phenoxy acetamide molecule AdipoRon has garnered attention as a potential cure for diseases like obesity, diabetes, heart disease, and nonalcoholic fatty liver disease.[6] Inflammation is often associated with pain perception, and there is a significant relationship between pain and inflammation. There is a pressing need for the creation of new anti-inflammatory and antinociceptive drugs because the side effects and lack of tolerability of existing therapies, including the nonsteroidal anti-inflammatory drugs (NSAIDs), limit their use.[7] Pain is the most common self-reported health condition in clinical practice and the community; nevertheless, suboptimal pain control is a worldwide issue. NSAIDs are indispensable for inflammation and pain management.[8] NSAIDs are essential for the management of inflammation and pain. However, recent research concerning paracetamol has necessitated a reevaluation of its application in clinical practice, underscoring the need to update existing clinical guidelines.[9] While newer pharmacological agents are designed to selectively inhibit COX-2, thereby reducing the production of prostaglandins and inflammatory mediators. Diclofenac is a well-known drug that acts on both COX enzyme isoforms. The utilization of NSAIDs is constrained by their adverse side effects, which include gastrointestinal toxicity, renal impairment, cardiovascular toxicity, and hepatic damage. Although the inhibition of COX-1 can adversely affect renal and gastric function, research suggests that COX-2 inhibition effectively manages inflammation. Conventional NSAIDs inhibit both enzymes, often resulting in gastrointestinal complications.[10] This has driven efforts to develop selective COX-2 inhibitors to overcome these limitations. In medicinal chemistry, incorporation of an amide moiety into chalcone scaffolds is a well-established strategy to enhance pharmacokinetic and pharmacodynamic properties, as amide linkers improve molecular recognition through hydrogen bonding and dipole interactions, and modulate solubility, lipophilicity, and metabolic stability.[11] Amide linkages not only increase hydrogen bonding potential with biological targets but also improve solubility, membrane permeability, and metabolic stability factors critical for effective drug action.[1,12] The amide group contributes significantly to ligand-target binding *via* dipole–dipole and hydrogen bonding interactions, which are crucial for improving specificity and potency in inflammation and pain-related pathways.[11] Furthermore, when fused with the chalcone backbone, the resulting amide-linked chalcone derivatives have demonstrated enhanced interaction with key enzymes such as cyclooxygenases and various cytokine regulators.[13] Recent reviews and experimental studies have highlighted the value of this amide-linked chalcone derivative design. Particularly, Alshazly and colleagues in 2025 presented a general overview of chalcone–acetamide derivatives, elucidating their wide spectrum of biological activities, such as anticancer, antimicrobial, antioxidant, and anti-inflammatory activities.[11] These derivatives not only retained the electrophilic Michael acceptor activity of chalcones but also gained superior binding affinity due to the amide functional group. Elkanzi and co-workers further reported that amide-linked chalcone derivatives exhibited marked inhibition of COX-2 and nitric oxide pathways, validating their utility in inflammation management.[1] Collectively, this structural integration is expected to enhance the selectivity, efficacy, and therapeutic index of chalcone-based drug candidates.[1] This study is of considerable importance because of its approach that integrates both computational and experimental strategies to design and evaluate novel chalcone derivatives as potential therapeutic candidates. Although chalcones are known for their extensive pharmacological potential, there remains a critical need for derivatives with enhanced potency and selectivity. By employing *in silico* docking analysis to investigate the molecular interactions with key biological targets, along with *in vivo* assessments of their anti-inflammatory and analgesic properties, this study offers a thorough evaluation of their therapeutic efficacy. This dual-faceted approach not only enhances our understanding of structure–activity relationships but also streamlines the drug discovery process, providing potential solutions to the ongoing challenges in pain and inflammation management.

2 Results and discussion

The novel chalcone derivatives were synthesized in three steps, as shown in Scheme 1.

Reagents and conditions: NaOH = sodium hydroxide; TEA = triethylamine; DCM = dichloromethane; DMF = dimethylformamide; anhy. K_2CO_3 = anhydrous potassium carbonate; KI = potassium iodide.

2.1 Chemistry

Eleven novel chalcone derivatives, (*E*)-*N*-(aryl)-2-(4″–(3‴–(2⁗-chlorophenyl)acryloyl) phenoxy)acetamide (**AS1-1–AS1-11**), were synthesized as shown in Scheme 1. The structures of these chalcone derivatives are detailed in the SI Data (Table S1). Initially, 4-hydroxy acetophenone (**1**) and 2-chlorobenzaldehyde (**2**) were reacted in ethanol with NaOH at 0 °C for 2–3 h to yield (*E*)-3-(2-chlorophenyl)-1-(4-hydroxyphenyl)prop-2-en-1-one with 87% yield. The compound (**3**), 2-chloro-*N*-arylacetamides (**6a–k**), and potassium carbonate were shaken together in dry DMF for 8 h at 50 °C to produce the target compounds, as indicated by Scheme 1. The reaction was followed through thin-layer chromatography (TLC). The products were precipitated on ice, filtered, dried, and recrystallized using methanol. The synthesized chalcone derivatives were characterized based on their physical properties, including molecular weight, melting point, and % yield, as summarized in (SI Data, Table S2).

The synthesis of the target molecules (**AS1-1–AS1-11**) was confirmed using Fourier transform infrared (FTIR) spectroscopy. The N–H stretching vibrations of the amide appeared at 3410–3276 cm^{-1}, and Csp^3-H stretches were observed at 2977–2920 cm^{-1}. Carbonyl stretches for ketone and amide appeared at 1703–1653 cm^{-1} and 1654–1588 cm^{-1}, respectively, while peaks for aromatic C=C, α,β-unsaturated systems, and C–Cl stretches appeared at 1594–1501 cm^{-1}, 1561–1436 cm^{-1} and 755–744 cm^{-1}, respectively. The synthesis of (*E*)-*N*-(aryl)-2-

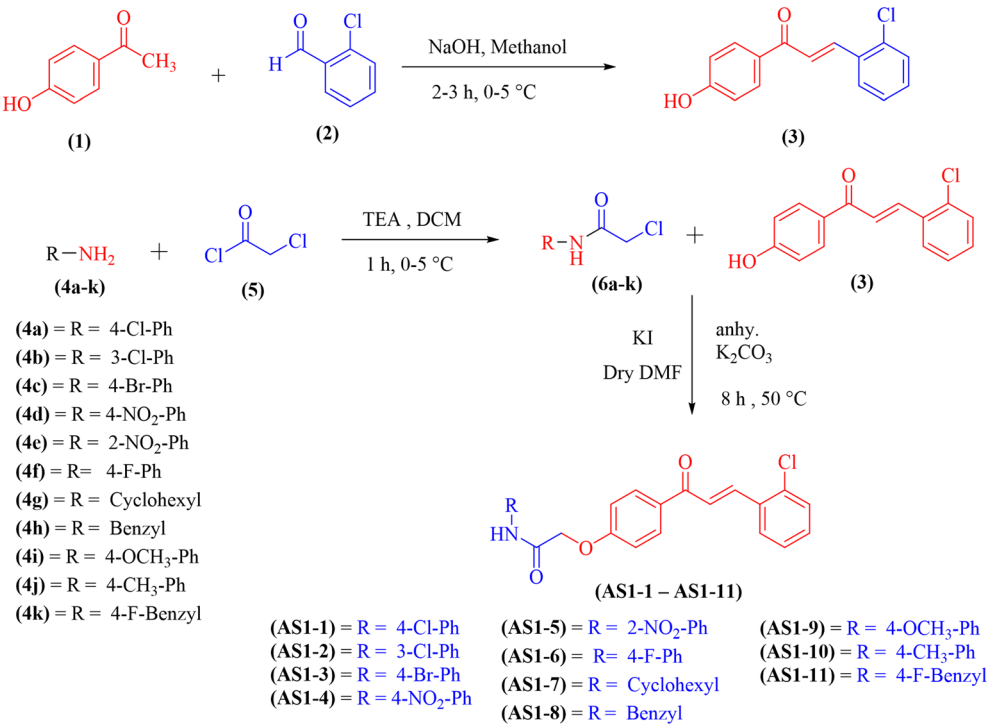

Scheme 1 General synthetic route for the synthesis of chalcone derivatives (AS1-1–AS1-11) through Claisen–Schmidt condensation.

(4″–(3‴–(2⁗-chlorophenyl)acryloyl)phenoxy)acetamide (**AS1-1–AS1-11**) was further confirmed using ^{1}H-NMR and ^{13}C-NMR spectroscopy. Methylene protons between the oxygen atom and carbonyl group resonated at 4.75–4.69 ppm, while the NH proton was seen as a singlet between 8.29 and 8.02 ppm. Additional confirmation came from the β-position proton (H-3‴) of the ketonic moiety at 8.20–8.10 ppm (doublet) and aromatic protons resonating at 8.31–6.89 ppm.

The synthesis of (*E*)-*N*-(aryl)-2-(4″-(3‴-(2⁗-chlorophenyl) acryloyl)phenoxy)acetamide (**AS1-1–AS1-11**) was verified through ^{13}C-NMR spectroscopy. The methylene carbon (C-2) exhibited resonance at 67.41–67.31 ppm, while the carbonyl carbons of the ketone (C-1″) and amide (C-1) were observed at 188.70–188.60 ppm and 165.50–164.21 ppm, respectively. Aromatic carbons were detected within the range of 160.56–114.19 ppm, with all other carbons resonating in their respective regions. The synthesis of the target compounds (**AS1-1–AS1-11**) was further corroborated using mass spectrometry. In the mass spectrum of **AS1-10**, the molecular ion peak (*m*/*z* (%) = 405.1) was identified as a radical cation, accompanied by isotopic peaks of ^{37}Cl and ^{81}Br, with the molecular ion peak serving as the base peak (100%). The fragment at *m*/*z* (%) 370.1 (86.2% abundance) likely resulted from the loss of a neutral chlorine atom, with additional fragment ion peaks observed, thus supporting the proposed fragmentation pattern.

2.2 *In vitro* toxicity analysis

2.2.1 Hemolytic assay. In accordance with the guidelines of the American Society for Testing and Materials (ASTM F756-00), a hemolytic study was performed to evaluate the toxicity of the recently synthesized chalcone derivatives to red blood cells. Hemolytic, slightly hemolytic, and non-hemolytic compounds were defined as those with hemolysis percentages greater than 5%, less than 5%, and less than 2%, respectively.[14] All newly synthesized chalcone derivatives (**AS1-1–AS1-11**) exhibited hemolysis percentages below 2%, classifying them as non-hemolytic. The hemolysis percentages ranged from 1.09% to 1.85%, indicating a minimal effect on erythrocyte membranes. The hemolytic activities of the newly synthesized chalcone derivatives (**AS1-1–AS1-11**) and the standard were compared with those of the negative control. The standard (Triton X-100) exhibited 98.2% hemolysis (***$P < 0.001$ *vs.* negative control), confirming its strong membrane-disrupting properties. At the same time, all chalcone derivatives showed non-significant hemolysis, comparable to the negative control, as shown in Fig. 1. This indicates their high biocompatibility and low cytotoxicity, which make these analogs safer for further evaluation and therapeutic applications. These findings suggest that the synthesized chalcone derivatives are highly safe in terms of red blood cell toxicity, making them promising candidates for further biological and pharmacological studies.

2.2.2 Brine shrimp lethality assay. The cytotoxic activity of the newly synthesized chalcone derivatives (**AS1-1–AS1-11**) was tested through the brine shrimp lethality assay. All tested compounds exhibited low cytotoxicity, with mortality percentages ranging from 43.3% to 46.6% at 80 μg mL^{-1} and 13.3% to 26.6% at 10 μg mL^{-1}. The lethal dose 50% (LD_{50}) values for all derivatives were greater than 200 μg mL^{-1}, indicating low toxicity. In contrast, the positive control doxorubicin showed high cytotoxicity with an LD_{50} of 8 μg mL^{-1}, whereas the

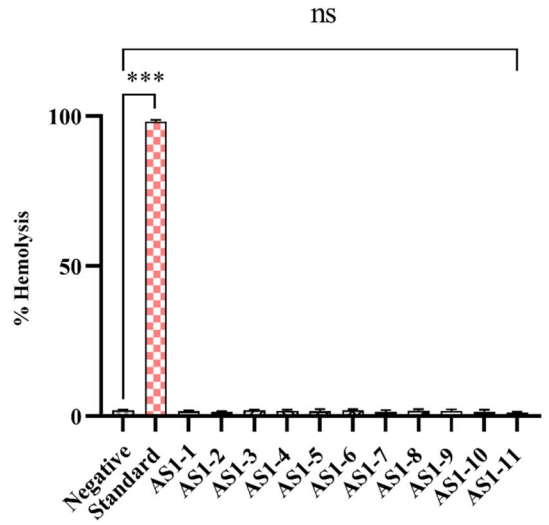

Fig. 1 Graphical representation of the hemolytic assay of newly synthesized chalcone derivatives (**AS1-1–AS1-11**) and standard compared to negative (phosphate-buffered saline, PBS). ***$P < 0.001$ *vs.* negative. The results are presented as the mean of triplicate ± standard deviation (SD) and were analyzed by one-way ANOVA followed by the LSD comparisons test. Standard = Triton X-100; PBS = phosphate-buffered saline; ns = non-significant.

negative control dimethyl sulfoxide (DMSO) exhibited no toxicity, as shown in Table 1. These results indicated that the synthesized chalcone derivatives have a good safety profile, making them promising candidates for further biological evaluation. Nevertheless, additional studies were needed to investigate their therapeutic potential.

2.2.3 Cytotoxicity assay (MTT assay). The newly synthesised chalcone derivatives (**AS1-1–AS1-11**) were screened for their cytotoxic activity against 3T3 fibroblast cells by the colorimetric assay 3-(4,5-dimethylthiazol-2-yl)-2,5-diphenyltetrazolium bromide (MTT). With the values lying between 3.78% and 21.63%, all compounds indicated only weak growth inhibition at the screening concentration of 30 μg mL^{-1} as summarized in Table 2. The tested derivatives were all considered inactive towards 3T3 cells, as none of them surpassed the pre-defined activity threshold of 50%. The reference drug, doxorubicin (30 μM), was used to validate the assay performance, which exhibited strong cytotoxicity and 95.8% inhibition with an IC_{50} of 0.17 ± 0.00 μM. These findings suggest that, at the dose measured, the chalcone analogues do not cause much damage to healthy fibroblast cells in a non-selective way. This is a good result from a therapeutic point of view as compounds that lack cytotoxicity against non-cancerous cell lines can give a less hazardous profile for further investigation in malignant cell models. In addition, as has also been established before for several chalcone templates, the inactivity in 3T3 cells does not exclude selective cytotoxicity in cancer-specific cell lines.[15] As per complementary studies, chalcone derivatives are often highly cytotoxic to cancer cells but non-toxic to normal cells. Chalcone derivatives, for instance, exhibited higher cytotoxicity against cancer cells compared to normal fibroblasts *in vitro* and *in vivo* studies, as per Ouyang *et al.* (2021).[16] In addition, Buso Bortolotto *et al.* (2014) discovered that some chalcone derivatives retained metabolic stability in animal models without inducing mild cytotoxicity in normal human cells. The concept that chalcone derivatives have the ability to exhibit selective cytotoxicity, targeting cancer cells without harming healthy, normal cells, is further reinforced by this finding.[17] Osmotic haemolysis tests delivered complementary evidence that chalcone derivatives were not damaging to the integrity of the erythrocyte membrane. Notwithstanding the cytotoxicity of the compounds against cancer cell lines, the reduction in haemolysis indicates that these chalcones are not toxic to erythrocytes, thereby supporting their biocompatibility.[18] Taken as a whole, these findings present convincing evidence that the derived chalcone derivatives are safe for healthy cells. Their potential as promising therapeutic options with virtually no adverse effects on normal tissues is underscored by their selective cytotoxicity.

2.2.4 *In vitro* cyclooxygenase isoenzymes (COX-1 and COX-2) inhibitory assay. A spectrophotometric microplate assay is

Table 1 Brine shrimp lethality assay with LD_{50} (μg mL^{-1}) of newly synthesized chalcone derivatives (**AS1-1–AS1-11**)

	% Mortality				
Compounds	80 μg mL^{-1}	40 μg mL^{-1}	20 μg mL^{-1}	10 μg mL^{-1}	LD_{50} (μg mL^{-1})
AS1-1	46.6 ± 4.71	36.6 ± 4.71	26.6 ± 4.71	16.6 ± 4.71	>200
AS1-2	43.3 ± 4.71	36.6 ± 4.71	26.6 ± 4.71	16.6 ± 4.71	>200
AS1-3	46.6 ± 4.71	33.3 ± 4.71	23.3 ± 4.71	23.3 ± 4.71	>200
AS1-4	43.3 ± 4.71	33.3 ± 4.71	23.3 ± 4.71	13.3 ± 4.71	>200
AS1-5	46.6 ± 4.71	36.6 ± 4.71	26.6 ± 4.71	16.6 ± 4.71	>200
AS1-6	46.6 ± 4.71	36.6 ± 4.71	26.6 ± 4.71	16.6 ± 4.71	>200
AS1-7	43.3 ± 4.71	36.6 ± 4.71	23.3 ± 4.71	16.6 ± 4.71	>200
AS1-8	43.3 ± 4.71	33.3 ± 4.71	23.3 ± 4.71	13.3 ± 4.71	>200
AS1-9	46.6 ± 4.71	36.6 ± 4.71	26.6 ± 4.71	23.3 ± 4.71	>200
AS1-10	46.6 ± 4.71	33.3 ± 4.71	26.6 ± 4.71	16.6 ± 4.71	>200
AS1-11	46.6 ± 4.71	36.6 ± 4.71	23.3 ± 4.71	16.6 ± 4.71	>200
Doxorubicin[a]	40 μg mL^{-1}	20 μg mL^{-1}	10 μg mL^{-1}	5 μg mL^{-1}	LD_{50} (μg mL^{-1})
	86.6 ± 5.77	76.6 ± 5.77	53.3 ± 5.77	36.6 ± 5.77	8
DMSO[b]	0	0	0	0	—

[a] Doxorubcin; positive control. [b] DMSO; negative control.

Table 2 Cytotoxicity assay (MTT assay) of newly synthesized chalcone derivatives against 3T3 cell lines[a]

Sample code	Conc. (μg mL^{-1}; 3T3)	% Inhibition/stimulation	$IC_{50} \pm SD$
AS1-1	30	5.01	Inactive
AS1-2	30	6.78	Inactive
AS1-3	30	12.77	Inactive
AS1-4	30	8.23	Inactive
AS1-5	30	4.5	Inactive
AS1-6	30	21.63	Inactive
AS1-7	30	8.17	Inactive
AS1-8	30	7.7	Inactive
AS1-9	30	11.05	Inactive
AS1-10	30	6.23	Inactive
AS1-11	30	3.78	Inactive
Doxorubicin (standard)	30 μM	95.8	0.17 ± 0.00

[a] The cut-off value is 50. Compounds below cut-off are all 'Inactive' on 3T3 cell lines.

typically employed to determine the inhibitory potential of synthesized chalcone derivatives (**AS1-1–AS1-11**) against both COX-1 and COX-2 isoforms. The parent chalcone scaffold displayed weak levels of inhibitory activity against both isoforms, with IC_{50} values of 21.5 ± 1.4 μM (COX-1) and 12.2 ± 0.8 μM (COX-2), corresponding to a selectivity index (SI) of 1.8 as shown in the Table 3. These values are in agreement with previous reports describing unsubstituted chalcones as weak or non-selective inhibitors of COX, consistent with their inherent absence of isoform preference. It was observed that a significant improvement in efficacy and selectivity was seen after structural modification by the introduction of an acetamide linker. This implies that slight chalcone backbone modifications could dramatically alter the binding orientation of the molecule within the COX active site and tip the balance in favor of COX-2 selectivity.[19] With COX-2 $IC_{50} = 2.7 \pm 0.2$ μM being considerably less than its COX-1 inhibition ($IC_{50} = 12.6 \pm 0.8$ μM), **AS1-6** was the best and most selective inhibitor of COX-2 among the synthesized chalcone analogs. It also possessed the highest selectivity index (SI = 4.7). This discrimination was considerably greater than that of the non-selective NSAID diclofenac sodium (SI = 1.6) and even compared favorably with the control COX-2 selective drug nimesulide (SI = 3.8). In addition, compounds **AS1-2** and **AS1-8** were found to exhibit strong selective inhibition of COX-2. Although **AS1-8** was found to inhibit COX-2 at 4.1 ± 0.3 μM *versus* 15.3 ± 1.0 μM for COX-1 (SI = 3.7), **AS1-2** inhibited COX-2 with an IC_{50} of 3.2 ± 0.3 μM *versus* COX-1 at 11.8 ± 0.9 μM. The prospects for reduced off-target gastrointestinal activity of the compounds are accentuated by their low micromolar COX-2 activity and notably worse COX-1 inhibition. These substituents most likely stabilize ligand binding by creating more secure contacts in COX-2's secondary pocket, which is absent in COX-1.[20] In addition, consistent with previous findings in which amide linkers improve binding affinity in heteroaryl chalcones,[19] the acetamide moiety could be contributing by forming hydrogen bonds that orient the chalcone nucleus in a more favorable direction towards COX-2 residues. Weaker selectivity (SI = 2.0–2.1) was exhibited by derivatives like **AS1-5**, **AS1-7**, and **AS1-11**, which suggests that extreme isoform preference demands a perfect balance between substituent position and electronic effects. Together, these outcomes indicate that **AS1-6**, **AS1-2**, and **AS1-8** represent the

Table 3 *In vitro* COX-1 and COX-2 inhibitory activity (IC_{50}, μM) of newly synthesized chalcone derivatives (AS1-1–AS1-11)

Compound	IC_{50} (μM, COX-1)	IC_{50} (μM, COX-2)	COX-2 selectivity index (SI)
Chalcone	21.5 ± 1.4	12.2 ± 0.8	1.8
AS1-1	19.4 ± 1.2	10.6 ± 0.8	1.8
AS1-2	11.8 ± 0.9	3.2 ± 0.3	3.7
AS1-3	22.7 ± 1.5	12.4 ± 0.9	1.8
AS1-4	28.3 ± 2.2	15.6 ± 1.3	1.8
AS1-5	16.7 ± 1.1	8.5 ± 0.7	2
AS1-6	12.6 ± 0.8	2.7 ± 0.2	4.7
AS1-7	26.5 ± 2.1	13.1 ± 1.0	2
AS1-8	15.3 ± 1.0	4.1 ± 0.3	3.7
AS1-9	18.6 ± 1.3	7.4 ± 0.5	2.5
AS1-10	16.2 ± 1.1	6.1 ± 0.4	2.7
AS1-11	17.1 ± 0.9	8.2 ± 0.6	2.1
Diclofenac sodium	7.4 ± 0.5	4.7 ± 0.3	1.6
Nimesulide	13.4 ± 0.9	3.5 ± 0.2	3.8

most viable leads of the series. Their improved selectivity profiles reflect the suitability of acetamide-substituted chalcones as safer alternatives for conventional NSAIDs as well as justify the design reasoning. The control inhibitors were assayed under similar conditions for comparison. The non-selective NSAID diclofenac sodium had mild inhibition of both isoforms (SI = 1.6), yet the selective COX-2 inhibitor nimesulide had higher preference (SI = 3.8). Notably, **AS1-6**'s selectivity (SI = 4.7) surpassed nimesulide, while that of **AS1-2** and **AS1-8** (SI = 3.7) was comparable and all surpassed diclofenac.

2.3 *In silico* ADMET evaluation

2.3.1 *In silico* absorption, distribution, metabolism, and excretion (ADME) assessment. The physicochemical and toxicity profiles of all synthesized chalcone derivatives were evaluated using Swiss ADME and Pharmacokinetics *via* Computational Structure-based Modeling (pkCSM) (SI Data, Table S3). Given the importance of ADMET evaluation in lead optimization, a software-based approach was employed to efficiently predict absorption, toxicity, and metabolism, thereby minimizing the necessity for costly *in vitro* and *in vivo* studies.[21] Lipophilicity, a critical physicochemical property, was evaluated using various logarithms of the partition coefficient between *n*-octanol (o) and water (w) ($\log P_{o/w}$) methodologies. The $\log P$ values for all compounds (**AS1-1–AS1-11**) were within an acceptable range, with the exception of **AS1-1**, **AS1-2**, and **AS1-3**. The overall average $\log P$ remained below 5 for the majority of the compounds, indicating their potential suitability for oral administration.[22] According to our results, the lipophilicity of chalcone derivatives and solubility were drug-like (SI Data, Tables S4 and S5). The chalcone derivatives (**AS1-1–AS1-11**) exhibited drug-like lipophilicity and moderate solubility, except for **AS1-1** to **AS1-3**, which showed lower solubility across the models, consistent with the data presented in Table S5.

Swiss ADME predicted high gastrointestinal (GI) absorption for all compounds, with **AS1-2**, **AS1-6**, and **AS1-11** showing the potential to cross barriers, while **AS1-1**, **AS1-3**, **AS1-4**, and **AS1-5** had lower blood–brain barrier permeability. P-glycoprotein (P-gp) substrate analysis revealed that **AS1-1** to **AS1-3**, **AS1-8**, **AS1-10**, and **AS1-11** are P-gp substrates, whereas the others are not. All compounds (**AS1-1–AS1-11**) exhibited inhibitory potential against Cytochrome P450 Family 1 Subfamily A Member 2 (CYP1A2), CYP3A4, CYP2C19, and CYP2C9, except **AS1-4**, **AS1-5**, and **AS1-7**, which lacked CYP1A2 inhibition, and only **AS1-7** showed CYP2D6 inhibition, and all compounds exhibited low skin permeability with $\log K_p > 2.5$.[23] The predicted pharmacokinetic parameters of all chalcone derivatives are summarized (SI Data, Table S6). All compounds adhered to the Lipinski and Ghose rules, except for **AS1-1** to **AS1-3**, each of which had a single Lipinski rule violation. Similarly, all compounds complied with Egan and Veber's rules, except **AS1-1**, which exhibited one violation of Egan's criteria. Additionally, all compounds showed only one violation of the Muegge rule for drug-likeness, with XLOGP3 values exceeding five (SI Data, Table S7).

2.3.2 Toxicity prediction. The pkCSM web server (http://biosig.unimelb.edu.au/pkcsm/) was employed to analyze the toxicity profiles of all compounds. The findings suggested that the synthesized compounds are likely to be safe. Most of the compounds (**AS1-1–AS1-11**) exhibited mutagenicity, except for **AS1-1**, **AS1-3**, and **AS1-7**, which were non-mutagenic. Additionally, **AS1-1** and **AS1-7** were non-carcinogenic.[24] Except for **AS1-7**, all compounds (**AS1-1–AS1-11**) were considered non-toxic to *Tetrahymena pyriformis* (SI Data, Table S8). **AS1-1** and **AS1-7** were predicted as non-carcinogenic in the pkCSM assessment; therefore, they do not appear in Table S8, which lists only the compounds flagged with carcinogenicity alerts. This clarification has been added to ensure transparency in data reporting.

2.4 Molecular docking studies

The docking analysis of the newly synthesized chalcone derivatives revealed binding affinities ranging from −6.7 to −8.4 kcal mol^{-1} for COX-1. The derivatives **AS1-2** and **AS1-8** demonstrated the highest affinities, with values of −8.4 and −8.3 kcal mol^{-1}, respectively, potentially attributable to halogen substitution. In contrast, **AS1-4** and **AS1-7** exhibited weaker affinities, measuring −6.7 and −6.8 kcal mol^{-1}, which

Table 4 Binding affinities and key molecular interactions of newly synthesized chalcone derivatives (AS1-1–AS1-11) with the COX-1 active sites compared to the standard drug, nimesulide

Compounds	Binding energies (kcal mol^{-1})	H-bond (amino acid residues)	π–π stacking (amino acid residues)	Additional interactions (amino acid residues)
AS1-1	−7.6	Hie90	Tyr355, Trp387, Tyr385	—
AS1-2	−8.4	—	Tyr355, Trp387, Tyr385	—
AS1-3	−7.0	—	—	Arg120 (Pi cation)
AS1-4	−6.7	Hie90	Trp387, Tyr385	—
AS1-5	−8	—	Tyr355, Trp387, Tyr385	Arg120, Glu524 (salt bridge)
AS1-6	−7.7	—	Tyr355, Trp387, Tyr385	—
AS1-7	−6.8	Glu524	Tyr355	
AS1-8	−8.3	—	Tyr355, Trp387, Tyr385	—
AS1-9	−7.0	Arg79	—	
AS1-10	−7.6	Glu A:524	—	Arg120 (Pi cation)
AS1-11	−7.6	Ser530, Ala527	Tyr355, Trp387	—
Nimesulide	−7.9	Arg120	Tyr355	—

may be attributed to substituent orientation or steric hindrance. Similarly, molecular docking of these chalcone derivatives against COX-2 indicated affinities between −7.9 and −10.2 kcal mol^{-1}. The derivatives **AS1-6** and **AS1-2** showed the strongest interactions, with affinities of −10.2 and −9.9 kcal mol^{-1}, likely due to the presence of electron-withdrawing groups. On the other hand, **AS1-10** and **AS1-9** exhibited −7.9 and −8.0 kcal mol^{-1} lower affinities, indicating the effect of electron-donating groups or weaker interactions with COX-2. Molecular docking analysis of the chalcone derivatives against COX-1 (PDB ID: 3N8X) and COX-2 (PDB ID: 1PXX) revealed varied binding affinities, as

Table 5 Binding affinities and molecular interaction profiles of the newly synthesized chalcone derivatives (**AS1-1–AS1-11**) with COX-2 compared to the standard drug, diclofenac sodium

Compounds	Binding energy (kcal mol^{-1})	H-bond (amino acid residues)	π–π stacking (amino acid residues)	Additional interactions (amino acid residues)
AS1-1	−9.6	—	Hie90	—
AS1-2	−9.9	—	Hie90	Tyr355 (halogen bond)
AS1-3	−8.4	—	Hie90	—
AS1-4	−8.5	—	—	Glu524, Arg120
AS1-5	−8.3	—	Hie90	—
AS1-6	−10.2	Tyr385, Ser530	Hie90, Tyr385, Trp387	—
AS1-7	−9.3	Ser530	—	Tyr355 (halogen bond)
AS1-8	−9.7	Tyr385, Ser530		—
AS1-9	−8.0	—	Hie90, Trp387, Tyr385	Ser530 (halogen bond)
AS1-10	−7.9	Leu352	Tyr355	—
AS1-11	−9.6	Arg120		
Diclofenac sodium	−8.1	Arg433, Asp515	—	Arg513, Arg433 (salt bridges), Arg433 (halogen bond)

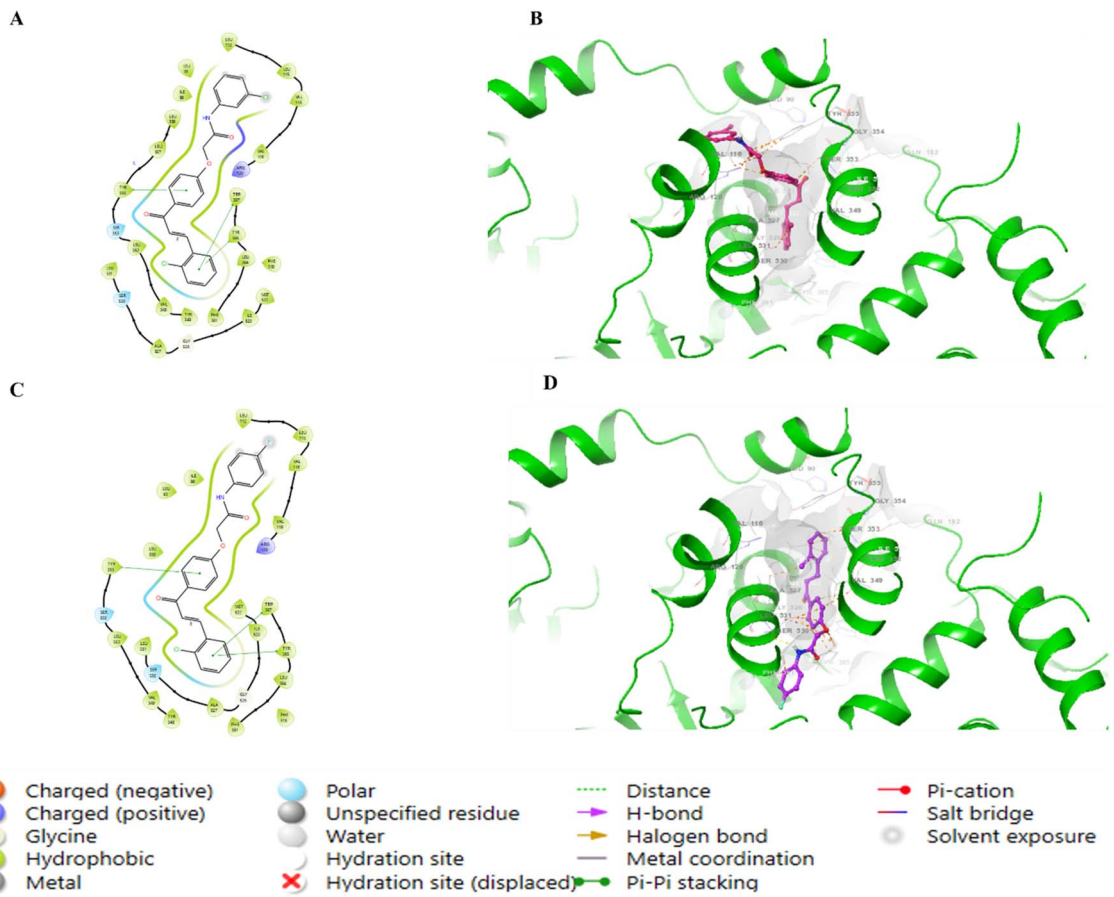

Fig. 2 2D and 3D molecular docking interactions of compound **AS1-2** (A and B) and **AS1-6** (C and D) against the COX-1 active sites.

presented in Tables 4 and 5. To ensure structural reliability in our molecular docking protocol, we employed literature-reported X-ray crystal structures of COX-1 (PDB ID: 3N8X) and COX-2 (PDB ID: 1PXX). These experimentally resolved protein models provide well-defined active-site conformations that enable accurate prediction of protein–compound interactions.

The 2D and 3D docking analyses of the compounds with the best docking score **AS1-2**, **AS1-6**, **AS1-8**, and **AS1-10**, against COX-1 identified strong interactions, including hydrogen bonding, π–π stacking, and additional interactions such as salt bridges and Pi-cation as demonstrated in Fig. 2 and 3, respectively. Hydrogen bonds were predominantly observed with residues such as Arg120, Arg79, Ser530, and Ala527, which are known to stabilize ligand binding within the COX-1 active sites. For instance, the carboxylate group of arachidonic acid forms a salt bridge with Arg120 and a hydrogen bond with Tyr355, underscoring the importance of these residues for ligand stabilization.[25] Salt bridges and Pi-cation with residues such as Glu524, Arg120, enhance ligand accommodation and potentially contribute to stronger affinity. Notably, π–π stacking interactions with Tyr355, Tyr385, and Trp387 facilitate π-electron delocalization, which improves ligand binding and stability. The reference drug, nimesulide, exhibited similar interactions, including hydrogen bonding with Arg120 and strong π–π stacking with the residue Tyr355, as shown in Table 5. The presence of multiple interactions between **AS1-2** and **AS1-6** suggests that these derivatives have potentially moderate affinity for COX-1, making them promising candidates for further evaluation.

The 2D and 3D molecular docking analysis of the highest docking score compounds **AS1-2**, **AS1-6**, **AS1-8**, and **AS1-10**, along with the reference drug diclofenac sodium against COX-2, revealed significant interactions within the active sites, including hydrogen bonding, π–π stacking, and additional interactions such as salt bridges and halogen as shown in Fig. 4–6, respectively. Hydrogen bonding predominantly involves residues such as Arg120, Arg433, Leu352, and Ser530, which stabilize the ligand–protein complex, and additional interactions such as salt bridges and halogen bond with Arg513, Arg433, Ser530, and Tyr355 enhance ligand positioning in the binding pocket. Additionally, π–π stacking with Hie90, Trp387, and Tyr385 contributes to the electron delocalization of the conjugated system, reinforcing the stability of the bound complex, as shown in Table 5. Diclofenac sodium formed interactions similar to those of the tested compounds, validating the docking protocol. The presence of key interactions in

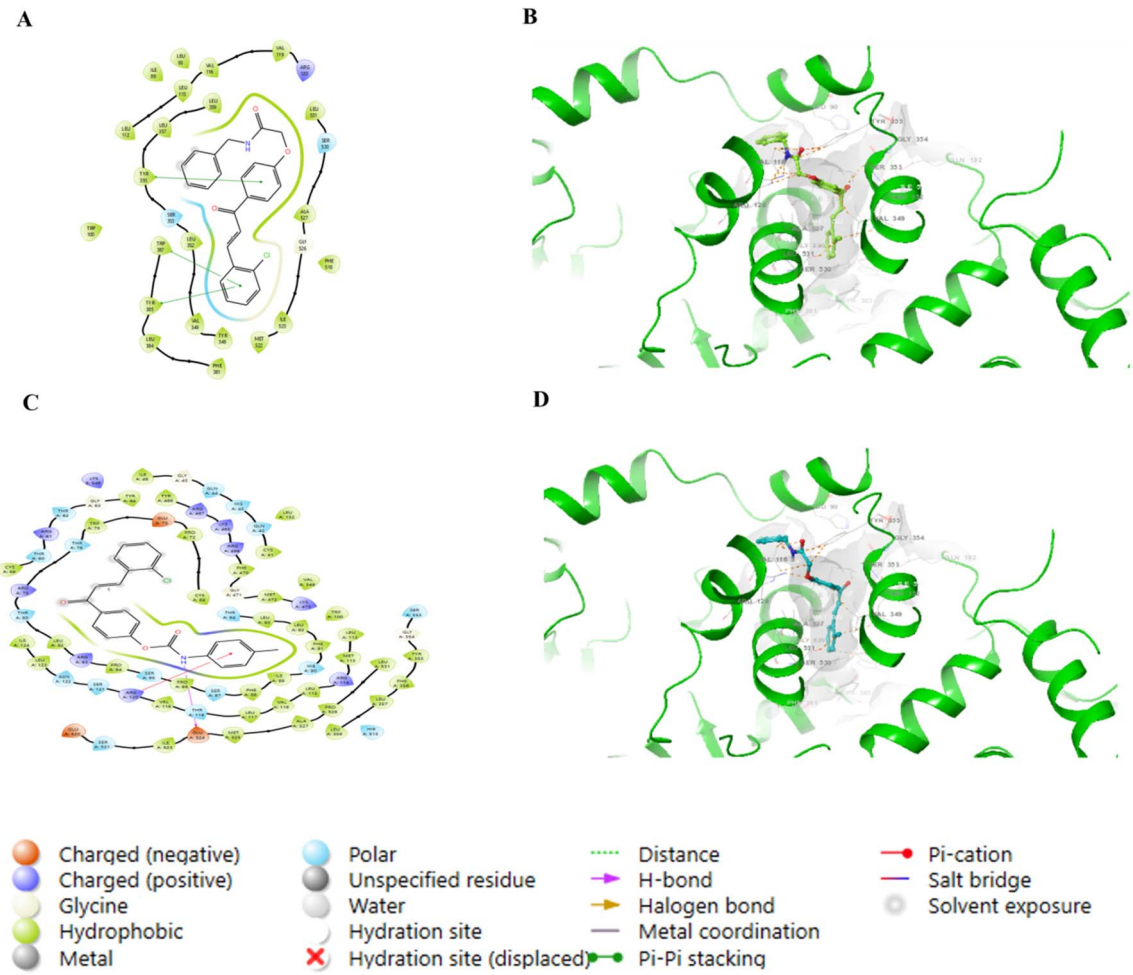

Fig. 3 2D and 3D molecular docking interactions of compound **AS1-8** (A and B) and **AS1-10** (C and D) against the COX-1 active sites.

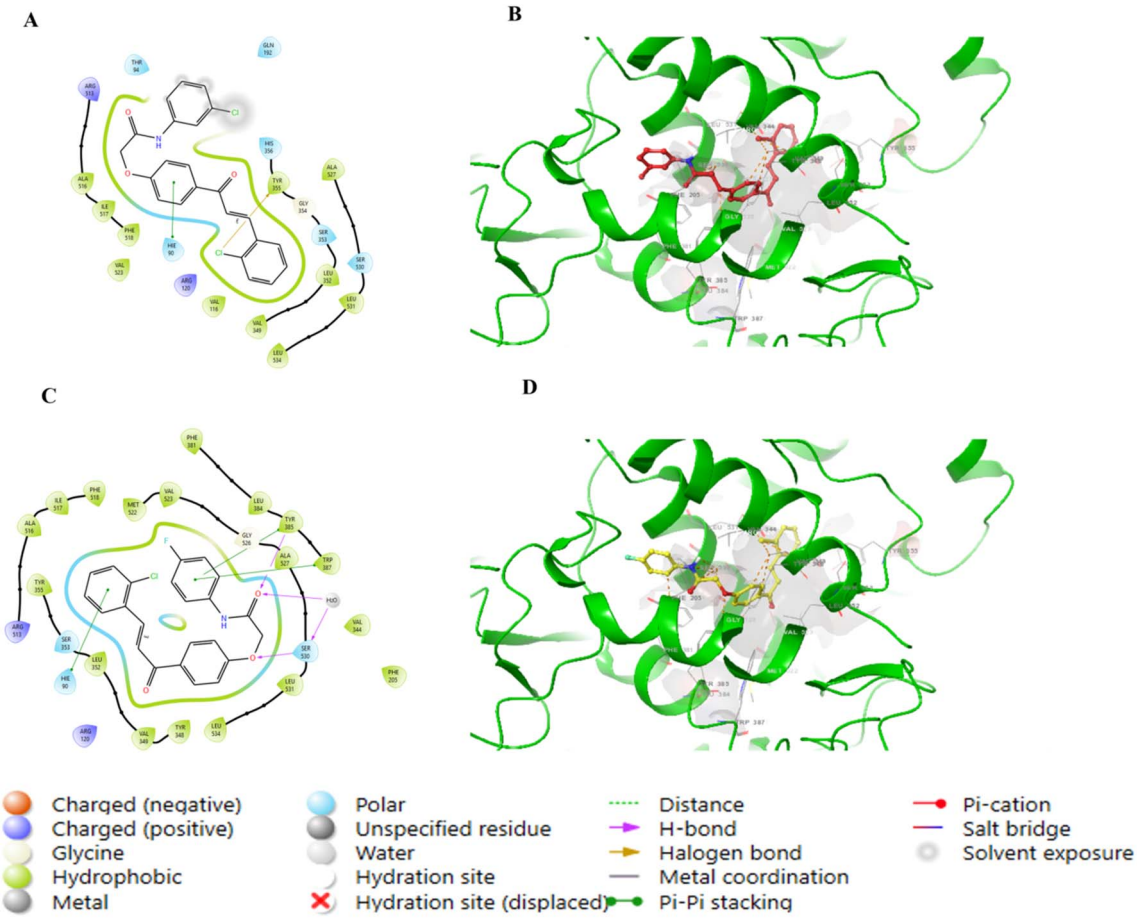

Fig. 4 2D and 3D molecular docking interactions of compound **AS1-2** (A and B) and **AS1-6** (C and D) against the COX-2 active sites.

compounds **AS1-2** and **AS1-6** suggests that these derivatives have potential COX-2 selectivity, warranting further biochemical and *in vitro* evaluations to confirm their inhibitory potential and selectivity index.

2.5 Molecular simulation

We employed molecular dynamics simulations together with structural interaction analysis to examine the protein–ligand complex stability and binding mechanism. The **AS1-6** was stabilized at the start of the simulation (0 ns) by hydrophobic interactions such as Val291 and hydrogen bonding with residues such as Phe210, Lys211, and Thr212 (Fig. 7a). The ligand was positioned deep in the binding pocket through these initial interactions. The **AS1-6** was still stably accommodated following a 100 ns simulation, though in a different orientation. Trp387, Leu294, Ala202, Gln203, Leu390, and Tyr409 were significant stabilising residues that together formed a robust network of hydrophobic and hydrogen bonding interactions (Fig. 7b). Although 2D interaction maps revealed long-lived major contacts with reorganization of particular hydrogen bonds and hydrophobic contacts as the system progressed (Fig. 7e and f), surface representations at both stages confirmed that the ligand was still buried within the pocket (Fig. 7c and d).

These results illustrate that while the interaction profile is dynamic, the entire binding is consistent over the course of the simulation. This stability was also complemented by the path of molecular dynamics (Fig. 8). Fig. 8a indicates that there were no considerable conformational changes throughout the 100 ns simulation, as the backbone RMSD values stabilized after about 20 ns and remained between 0.3 and 0.4 Å. As evidenced by the constant radius of gyration (2.45–2.50 Å) (Fig. 8b), the compactness of the protein was kept intact. Hydrogen bond analysis indicated that while the number of protein–ligand hydrogen bonds varied, interactions were present at all times (Fig. 8c), indicating a dynamic yet persistent mode of binding. RMSF analysis identified localized flexibility in loop areas, but the residues around the binding pocket were relatively rigid (Fig. 8d) supporting the persistence of ligand interactions. Together, these findings show that the **AS1-6** is firmly anchored within the active site of the protein throughout the simulation. Stability of the interaction network, along with retained structural compactness of the protein, unequivocally argues in favor of the stability of the complex.

2.6 *In vivo* behavioural studies

The anti-inflammatory and antinociceptive properties of the novel chalcone derivatives **AS1-1–AS1-11** were also investigated in this study. Tissue damage causes acute pain, which is exacerbated by inflammation and mediators such as prostaglandins, making nociceptors more sensitive.[26] Diclofenac

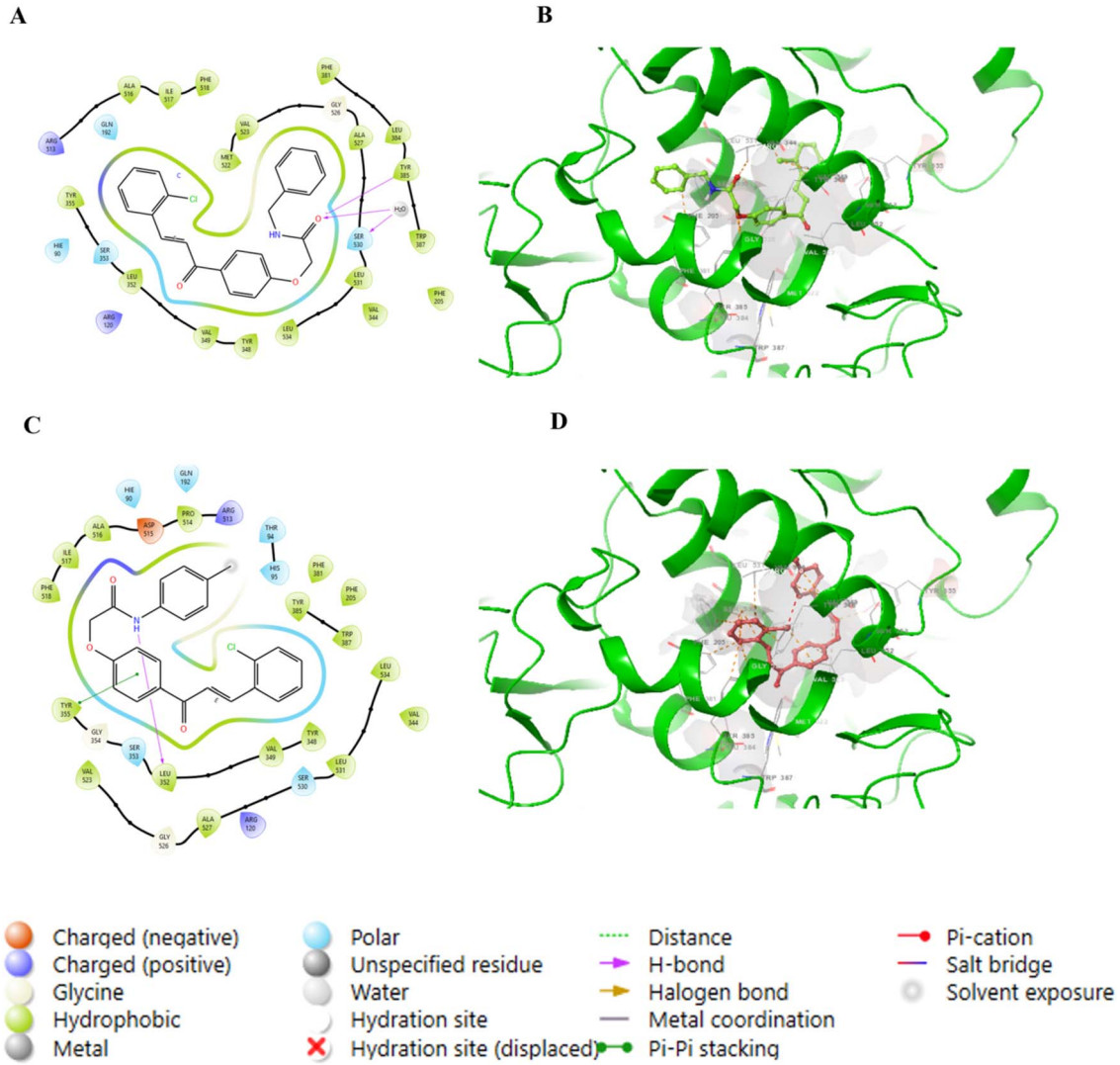

Fig. 5 2D and 3D molecular docking interactions of compound **AS1-8** (A and B) and **AS1-10** (C and D) against the COX-2 active sites.

potassium and ibuprofen are examples of NSAIDs that decrease inflammation by blocking COXs and modifying nociceptor sensitivity, aiding pain management.[27] Central mechanisms, such as the descending inhibitory pathway, contribute to the effects of NSAIDs, including indomethacin.[28] Medications that target multiple mechanisms are advantageous for the management of pain and inflammation. Eleven chalcone derivatives were synthesized for this study, and their effectiveness was evaluated using carrageenan-induced paw edema, formalin-induced paw licking, and acetic acid-induced writhing test.[29–31]

2.6.1 Acetic acid-induced writhing test. *In vivo* antinociceptive activity is commonly evaluated using the writhing test induced by acetic acid. This method is particularly sensitive for detecting the efficacy of NSAIDs and centrally acting analgesics.[32] Endogenous chemicals that irritate painful nerve endings are released when acetic acid is administered, resulting in characteristic writhing movements in experimental animals.

The mean number of writhes in normal, negative, standard, and newly synthesized chalcone derivatives (**AS1-1–AS1-11**) were 3 ± 0.81, 40 ± 0.63, 20 ± 0.81, 30 ± 0.81, 18 ± 0.81, 28 ± 0.81, 27 ± 0.81, 29 ± 0.81, 17 ± 0.81, 28 ± 0.81, 19 ± 0.81, 18.6 ± 1.24, 16.6 ± 1.24, 27 ± 0.81, respectively. The antinociceptive properties of chalcone derivatives are largely influenced by the type and position of substituents. **AS1-2** (3′–Cl–Ph), **AS1-6** (4′–F–Ph), and **AS1-9** (4′-methoxy) displayed the highest activities, which may be due to their favorable electronic effects, lipophilicity, and strong receptor interactions. These findings align with previous studies reporting that chalcone derivatives exhibit analgesic and anti-inflammatory activities, and suggest that structural and physicochemical factors, such as lipophilicity and electronic properties, may influence activity.[33] **AS1-4** (4′–NO_2–Ph) and **AS1-5** (2′–NO_2–Ph) exhibited weaker effects because their high polarity reduced membrane permeability. **AS1-1** (4′–Cl–Ph) was less effective than **AS1-2** (3′–Cl–Ph), suggesting that *meta*-substitution enhances receptor binding, consistent with structure–activity relationship studies indicating that substitution patterns significantly affect biological activity.[34]

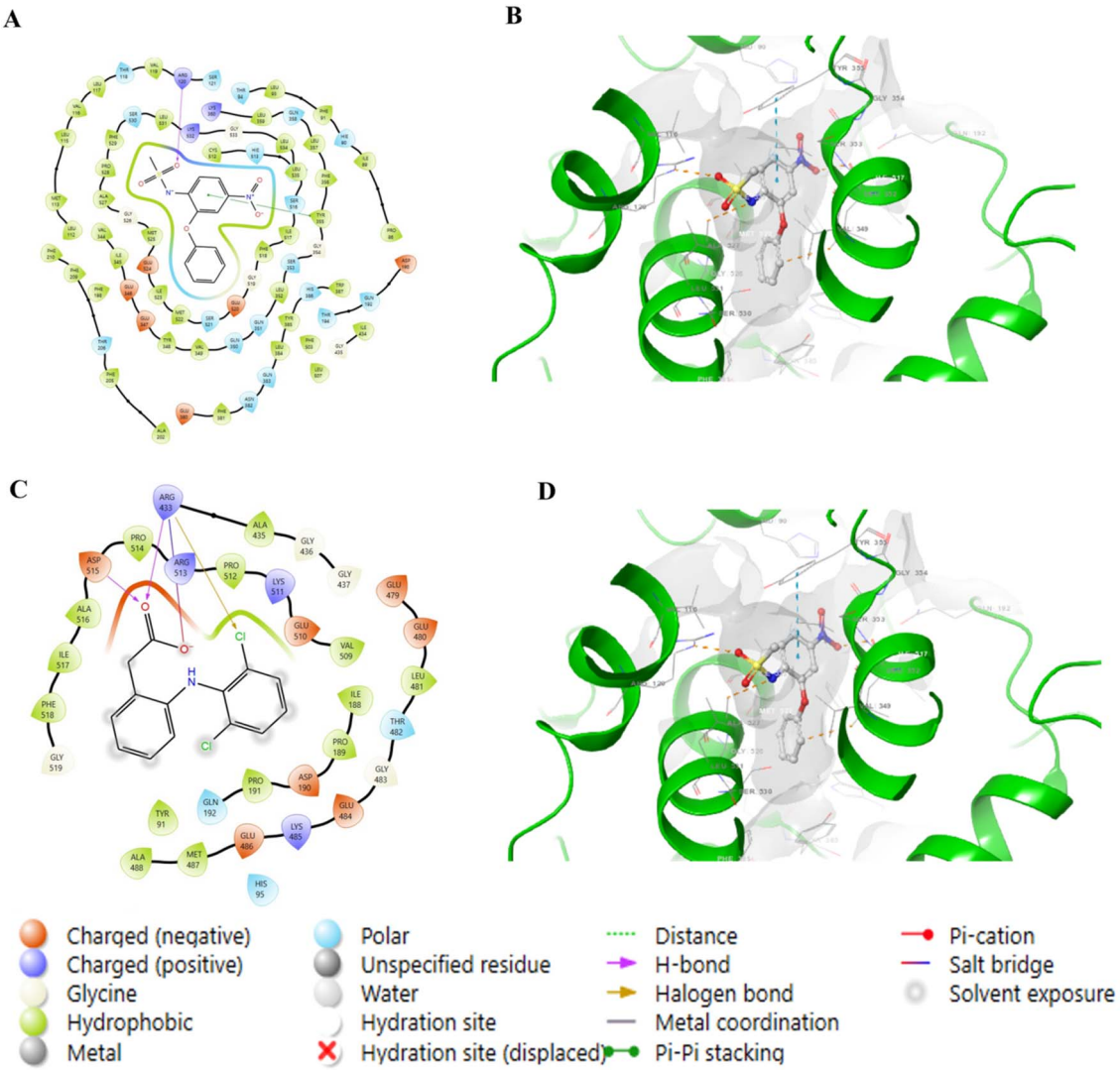

Fig. 6 2D and 3D molecular docking interactions of standard drugs Nimesulide (A and B) and diclofenac sodium (C and D) against COX-1 and COX-2 active site respectively.

Administration of the newly synthesized chalcone derivatives (**AS1-1–AS1-11**; 10 mg kg^{-1}, i.p.) and the standard drug diclofenac sodium (10 mg kg^{-1}, i.p.) significantly reduced (**$P < 0.001$) the number of writhes compared with the negative control group. Additionally, the negative control group exhibited a substantial increase in writhing responses compared to the normal control group ($^{\#\#\#}P < 0.001$), confirming the efficacy of acetic acid in inducing nociceptive behavior (Fig. 9). The observed antinociceptive effects of chalcone derivatives suggest their potential in modulating pain pathways.

2.6.2 Formalin-induced paw licking test. The formalin-induced paw licking test is a well-established method for evaluating both neurogenic (early phase) and inflammatory (late phase) pain responses in animal models. In this study, the mean durations of paw licking/biting (in seconds) during phase I (early phase) for normal, negative control, standard (diclofenac sodium), and newly synthesized chalcone derivatives (**AS1-1–AS1-11**) were 4.3 ± 0.47, 64 ± 0.81, 23.6 ± 2.05, 42 ± 0.81, 26.3 ± 1.24, 51 ± 0.81, 51 ± 0.81, 56 ± 0.81, 25 ± 0.81, 59 ± 0.81, 33 ± 0.81, 50 ± 0.81, 24 ± 1.63, and 50 ± 0.81, respectively. For phase II (late phase), the corresponding values were 11 ± 0.81, 219 ± 0.81, 106.6 ± 1.24, 150 ± 4.08, 106.6 ± 1.69, 171.6 ± 6.23, 143.3 ± 4.92, 182 ± 2.94, 105 ± 1.63, 185 ± 4.08, 135 ± 8.16, 184.6 ± 5.55, 106 ± 1.63, and 181 ± 5.35. These results indicate that certain chalcone derivatives, particularly **AS1-2** (3′–Cl–Ph), **AS1-6** (4′–F–Ph), and **AS1-10** (4′–CH_3–Ph), exhibited significant antinociceptive effects in both phases of the formalin test.

The antinociceptive potential of the chalcone derivatives in the formalin test was influenced by the electronic properties and lipophilicity of the substituents. Compounds **AS1-2**, **AS1-6**, and **AS1-10** demonstrated the strongest pain-relieving effects, likely due to their enhanced receptor interactions and membrane permeability. Specifically, the *meta*-positioned chlorine in **AS1-2** and *para*-fluorine in **AS1-6** may improve receptor binding, whereas the methyl group in **AS1-10** may contribute to better lipophilic interactions. These findings align with those of previous studies, indicating that small substituents at the para position of the phenyl ring enhance

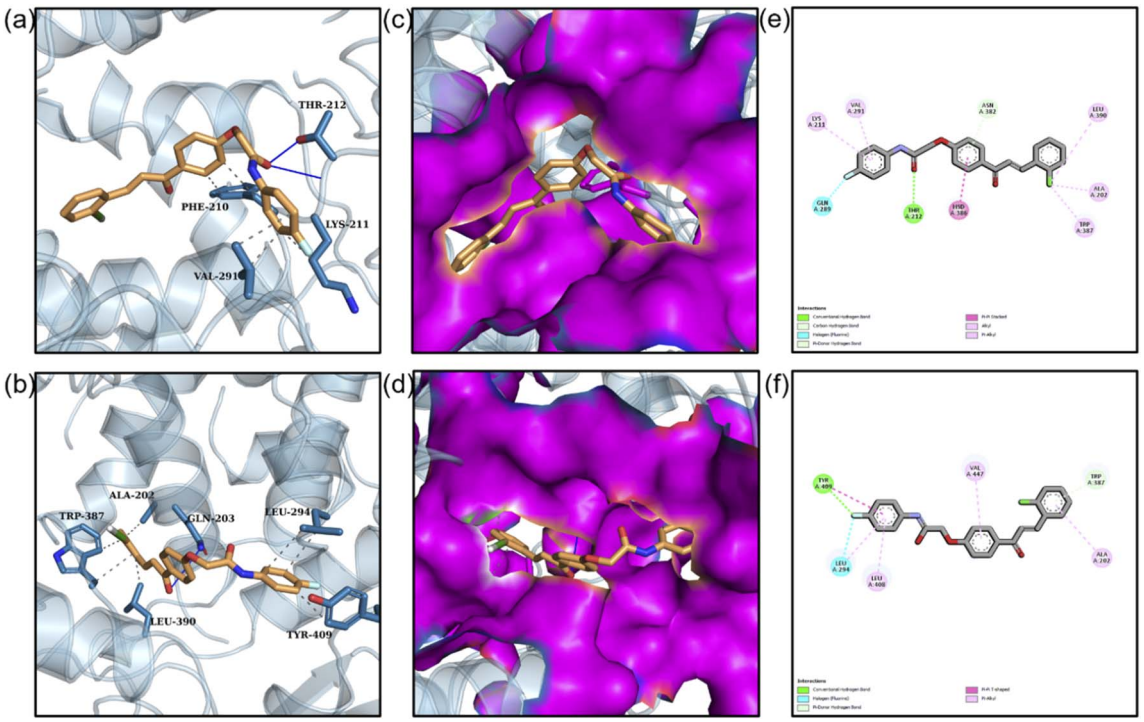

Fig. 7 Demonstrates the binding interactions of the ligand (**AS1-6**) with the target protein at the beginning (0 ns) and end (100 ns) of the molecular dynamics simulation. (a and b) Principal hydrogen bonds and hydrophobic contacts are shown in this three-dimensional stick model of ligand–protein interactions at 0 ns (a) and 100 ns (b). (c and d) Surface representation showing conformational change in cavity access during the simulation, with the ligand placed inside the binding pocket at 0 ns (c) and 100 ns (d). (e and f) Two-dimensional interaction diagrams of ligand-residue contacts at 0 ns (e) and 100 ns (f) that show the π–π interactions, hydrophobic interactions, and hydrogen bonds with neighbouring residues. When combined, these panels show how ligand binding inside the active site has changed and remained stable during the simulation timescale.

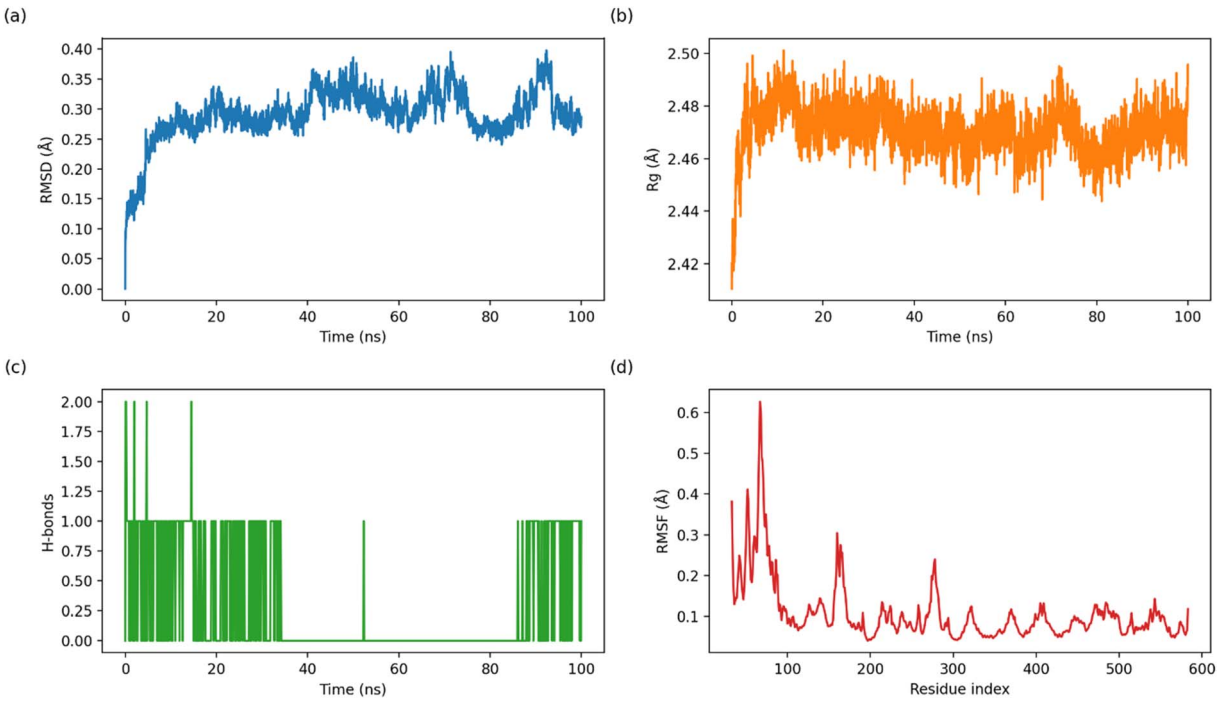

Fig. 8 Comparative binding interactions of the ligand with the target protein at the beginning (0 ns) and the end (100 ns) of the molecular dynamics simulation. (a) The root mean square deviation (RMSD) of the protein backbone, which shows the structural stability overall throughout the simulation. (b) The radius of gyration (R_g) of the protein, which reflects the stability and compactness of the complex while folding. (c) The number of hydrogen bonds formed between the protein and ligand within the simulation time represents the stability of the connection. (d) Root mean square fluctuation (RMSF) of protein residues, which indicates the stable and flexible regions of the structure.

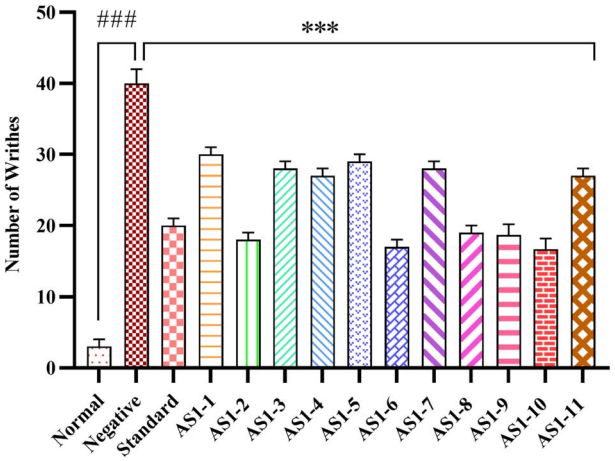

Fig. 9 Antinociceptive effects of newly synthesized compounds (**AS1-1–AS1-11**; 10 mg kg^{-1}) and standard (diclofenac sodium; 10 mg kg^{-1}) against acetic acid-induced writhing. $^{###}P < 0.001$ *vs.* normal. $^{***}P < 0.001$ *vs.* negative. Data are expressed as mean ± SD ($n = 3$) and analyzed using one-way ANOVA followed by the LSD comparisons test.

antinociceptive activity, whereas bulkier groups may reduce efficacy.[35]

In comparison to the negative control, the administration of the newly synthesised chalcone derivatives (**AS1-1–AS1-11**; 10 mg kg^{-1}, i.p.) and the standard drug diclofenac sodium (10 mg kg^{-1}, i.p.) substantially reduced the paw licking response in both phases ($^{***}P < 0.001$). The negative control group exhibited a significantly ($^{###}P < 0.001$) higher number of licking responses than the normal group (Fig. 10), confirming the validity of formalin-induced nociception. These observations suggest that halogenated and small lipophilic substituents are key contributors to the analgesic effects of chalcone derivatives, making **AS1-2**, **AS1-6**, and **AS1-10** promising candidates for further study.

2.6.3 Carrageenan-induced paw edema test. The anti-inflammatory effects of the newly synthesized chalcone derivatives were evaluated using the carrageenan-induced paw edema test. This test is a popular method for assessing acute inflammation.[36–38] Table 6 presents the anti-inflammatory effects of the newly synthesized chalcone derivatives (**AS1-1–AS1-11**) and the standard drug, diclofenac sodium (10 mg kg^{-1}), on carrageenan-induced paw edema in mice. The paw thickness was recorded at different time intervals (0–5 h) to assess the reduction in inflammation. The negative control group exhibited a continuous increase in paw thickness, reaching 5.00 ± 0.04 mm at 5 h, confirming significant inflammation. This observation aligns with previous studies that have established carrageenan as a potent inducer of localized inflammatory responses through COX-mediated prostaglandin synthesis.[39] In contrast, the administration of diclofenac sodium significantly inhibited edema formation, reducing paw thickness to 3.7 ± 0.08 mm at 5 h ($^{***}P < 0.001$) *vs.* negative control, confirming its potent anti-inflammatory effect. Among the chalcone derivatives, **AS1-2** reduced paw thickness to 3.8 ± 0.08 mm at 5 h, exhibiting a strong anti-inflammatory response. Similarly, **AS1-6** showed 4.00 ± 0.08 mm at 5 h, which was comparable to diclofenac sodium, while **AS1-8** resulted in 3.93 ± 0.12 mm at 5 h, also indicating significant anti-inflammatory activity. The observed anti-inflammatory properties of these chalcone derivatives may be attributed to their ability to inhibit cyclooxygenase (COX) enzymes, thereby suppressing prostaglandin synthesis, a key mechanism in inflammation.[40] Fig. 11 shows the progression of paw edema in the different treatment groups over 5 h. The negative control group showed a significant increase in paw thickness compared to the normal control group ($^{###}P < 0.001$), highlighting the effectiveness of carrageenan in inducing inflammation. However, the administration of diclofenac sodium and selected chalcone derivatives (**AS1-2**, **AS1-6**, and **AS1-8**) significantly reduced paw swelling compared to that in the negative control group ($^{***}P < 0.001$),

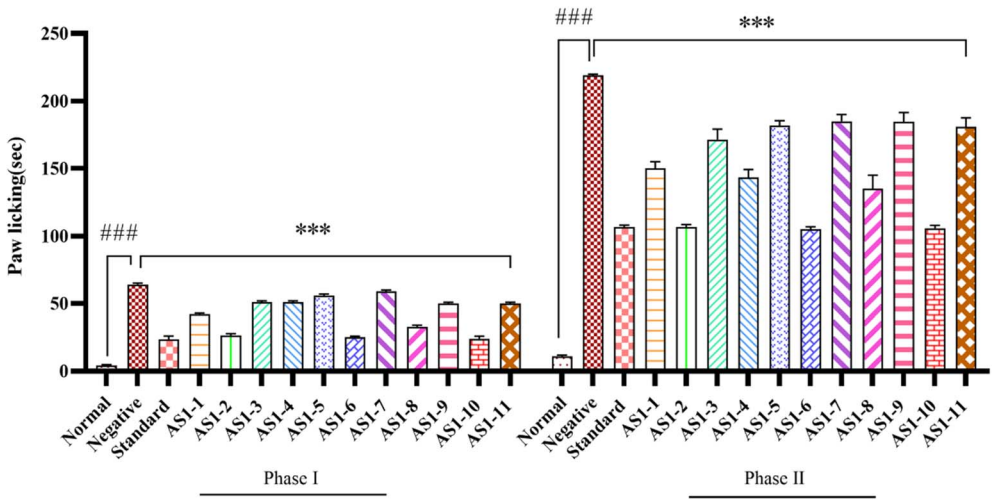

Fig. 10 Antinociceptive effects of newly synthesized chalcone derivatives (**AS1-1–AS1-11**; 10 mg kg^{-1}) and standard (diclofenac sodium; 10 mg kg^{-1}) against formalin-induced paw licking. $^{###}P < 0.001$ *vs.* normal. $^{***}P < 0.001$ *vs.* negative. Data are expressed as mean ± SD ($n = 3$) and analyzed using one-way ANOVA followed by the LSD comparisons test.

Table 6 Paw edema volume (mm) measurements of newly synthesized chalcone derivatives (**AS1-1–AS1-11**) in the carrageenan-induced paw edema model in mice. The table presents the anti-inflammatory effects of each compound based on paw thickness reduction compared to the negative control group, indicating their potential efficacy in inhibiting acute inflammation

Time (h)	Normal control	Negative control	Standard (diclofenac sodium)	AS1-1	AS1-2	AS1-3	AS1-4	AS1-5	AS1-6	AS1-7	AS1-8	AS1-9	AS1-10	AS1-11
0 h	3.46 ± 0.04	3.46 ± 0.04	3.53 ± 0.04	3.4 ± 0.04	3.36 ± 0.04	3.43 ± 0.04	3.43 ± 0.04	3.36 ± 0.04	3.43 ± 0.04	3.4 ± 0.08	3.4 ± 0.08	3.4 ± 0.08	3.46 ± 0.04	3.3 ± 0.08
1 h	3.46 ± 0.04	4.96 ± 0.04	4.26 ± 0.04	4.53 ± 0.04	4.33 ± 0.04	4.73 ± 0.04	4.76 ± 0.04	4.76 ± 0.04	4.66 ± 0.04	4.7 ± 0.08	4.56 ± 0.04	4.7 ± 0.08	4.76 ± 0.04	4.71 ± 0.04
2 h	3.46 ± 0.04	5.06 ± 0.04	4.16 ± 0.12	4.33 ± 0.04	4.23 ± 0.04	4.7 ± 0.08	4.66 ± 0.04	4.66 ± 0.04	4.53 ± 0.04	4.63 ± 0.04	4.5 ± 0.08	4.6 ± 0.08	4.56 ± 0.04	4.6 ± 0.08
3 h	3.46 ± 0.04	5.06 ± 0.04	4.06 ± 0.09	4.2 ± 0.08	4.1 ± 0.08	4.46 ± 0.04	4.56 ± 0.04	4.6 ± 0.08	4.33 ± 0.04	4.33 ± 0.04	4.23 ± 0.12	4.36 ± 0.04	4.43 ± 0.04	4.43 ± 0.04
4 h	3.5 ± 0.04	5.13 ± 0.04	3.8 ± 0.08	4.16 ± 0.04	3.9 ± 0.08	4.26 ± 0.12	4.36 ± 0.04	4.3 ± 0.08	4.1 ± 0.08	4.2 ± 0.08	4.03 ± 0.12	4.2 ± 0.08	4.23 ± 0.04	4.24 ± 0.12
5 h	3.46 ± 0.04	5.00 ± 0.04	3.7 ± 0.08	4.06 ± 0.04	3.8 ± 0.08	4.16 ± 0.12	4.26 ± 0.04	4.2 ± 0.08	4.00 ± 0.08	4.06 ± 0.04	3.93 ± 0.12	4.1 ± 0.08	4.13 ± 0.04	4.14 ± 0.12

demonstrating their potential anti-inflammatory effects. Notably, **AS1-2** and **AS1-6** exhibited comparable efficacy to diclofenac sodium, suggesting their potential as COX inhibitors.

Recent research indicates that cyclooxygenase (COX) inhibition is not the only mechanism by which chalcones have shown anti-inflammatory properties, but may also involve modulation of multiple intracellular pathways. Nuclear factor kappa B (NF-κB), a crucial transcriptional regulator of pro-inflammatory cytokines such as IL-1β and TNF-α, has been shown to be inhibited by derivatives of chalcone.[41] They also inhibit the expression of inducible nitric oxide synthase and reduce nitric oxide production, which contributes to oxidative stress and inflammatory progression.[42,43] Additionally, chalcones can regulate mitogen-activated protein kinase (MAPK) cascades, namely ERK, JNK, and p38 pathways, affecting cytokine release and cellular responses to inflammatory stimuli.[44] Notably, some chalcones downregulate the activation of the NLRP3 inflammasome, a multiprotein complex involved in caspase-1 activation and IL-1β maturation.[45] These multifactorial effects may contribute collectively to the anti-inflammatory and antinociceptive activity observed *in vivo* in this study.

2.7 *Ex vivo* anti-inflammatory assay

2.7.1 Enzyme-linked immunosorbent assay (ELISA) for COX-2. The observed reduction in COX-2 levels by the chalcone derivatives (**AS1-2**, **AS1-6**, and **AS1-8**) is consistent with the reported anti-inflammatory potential of chalcone scaffolds as depicted in Fig. 12 The α,β-unsaturated carbonyl system, the main pharmacophore of chalcones, is responsible for their inhibitory effects on inflammation, including suppression of NF-κB signaling and modulation of pro-inflammatory cytokines such as TNF-α, IL-1β, IL-6, and IL-8.[46,47] Recent evidence further highlights that chalcone derivatives can activate the Nrf2/ARE redox-sensitive pathway, thereby enhancing antioxidant defenses and mitigating oxidative stress-driven inflammation.[48] Such multi-targeted activity provides chalcones with a broader therapeutic profile compared to conventional NSAIDs like diclofenac, which primarily act through COX inhibition. In this study, the tested derivatives produced a measurable decline in COX-2 expression compared to the negative control, and their promising activity was closely comparable to that of the standard NSAID diclofenac. The potent anti-inflammatory activity of the tested chalcone derivatives can be attributed to the electron-withdrawing halogen substituents (Cl, F), which enhance the electrophilic character of the α,β-unsaturated carbonyl system and optimize interactions within the COX-2 active site. Notably, *meta*-Cl (**AS1-2**) and *para*-F (**AS1-6**) substitutions confer favorable electronic and halogen interactions. Chalcones bearing fluoride or chloride groups have been reported to display superior anti-inflammatory potency, in some instances exceeding standard NSAIDs such as indomethacin and ibuprofen, underscoring the pivotal role of electron-withdrawing groups (EWGs) in modulating bioactivity.[49] In the case of **AS1-8**, the unsubstituted benzyl ring and flexible linker may allow optimal π–π stacking and hydrogen bonding interactions within the COX-2 binding pocket, resulting in activity

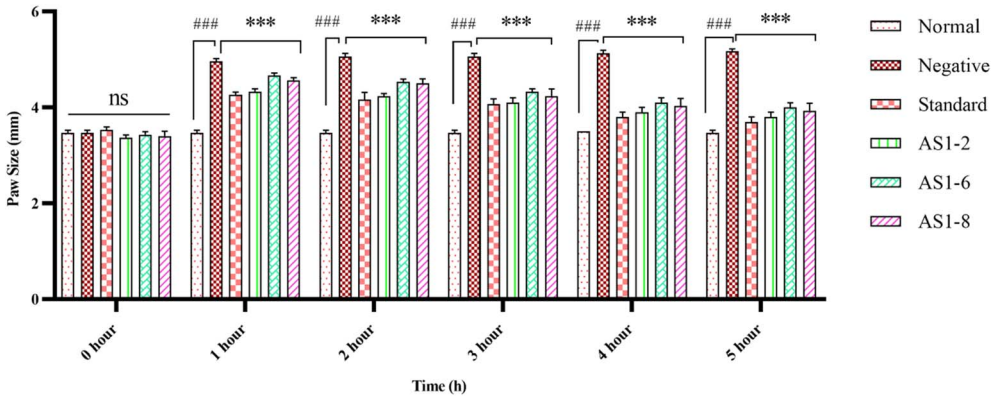

Fig. 11 Anti-inflammatory effects of newly synthesized chalcone derivatives (**AS1-2**, **AS1-6**, **AS1-8**; 10 mg kg^{-1}) and standard (diclofenac sodium; 10 mg kg^{-1}) against carrageenan-induced paw edema. $^{###}P < 0.001$ *vs.* normal. $^{***}P < 0.001$ *vs.* negative. Data are expressed as mean ± SD ($n = 3$) and analyzed using two-way ANOVA pairwise comparison test. ns = non-significant.

comparable to the halogen-substituted derivatives (**AS1-2** and **AS1-6**). Additionally, the amide linkage enhances hydrogen bonding potential and metabolic stability, collectively contributing to the robust pharmacological profile of these derivatives. Importantly, the absence of significant COX-2 upregulation in the normal control further validates the specificity of the inflammatory response observed in the negative control. Together, these findings suggest that the synthesized chalcone derivatives possess anti-inflammatory potential, with possible advantages in safety compared to standard NSAIDs.

2.8 Structure–activity relationship

The impact of various substitutions on biological activities was demonstrated by structure–activity relationship (SAR) analysis of the synthesized chalcone derivatives. All compounds were non-hemolytic, confirming their biocompatibility, and exhibited LD_{50} values above 200 μg mL^{-1} in the brine shrimp lethality assay, suggesting low cytotoxicity. In analgesic and anti-inflammatory models, **AS1-2** (3–Cl–Ph), **AS1-6** (4–F–Ph), and **AS1-10** (4–CH_3–Ph) demonstrated the most potent effects in both acetic acid-induced writhing and formalin-induced paw licking tests, comparable to the standard, likely because of their balanced lipophilicity and electronic effects that facilitate enzyme interactions. In the carrageenan-induced paw edema test, **AS1-2**, **AS1-6**, and **AS1-8** exhibited the highest anti-inflammatory activity, indicating that halogen and benzyl substitutions play crucial roles in stabilizing interactions with inflammatory mediators. The variation in activity suggests that electron-withdrawing groups (Cl, F) enhance anti-inflammatory effects by modulating COX inhibition. The benzyl substitution in **AS1-8** likely facilitated π–π stacking interactions, enhancing anti-inflammatory efficacy. Overall, the SAR findings suggest that halogenated derivatives (**AS1-2** and **AS1-6**) and hydrophobic substitutions (**AS1-8** and **AS1-10**) significantly contribute to the observed pharmacological activities (Fig. 13).

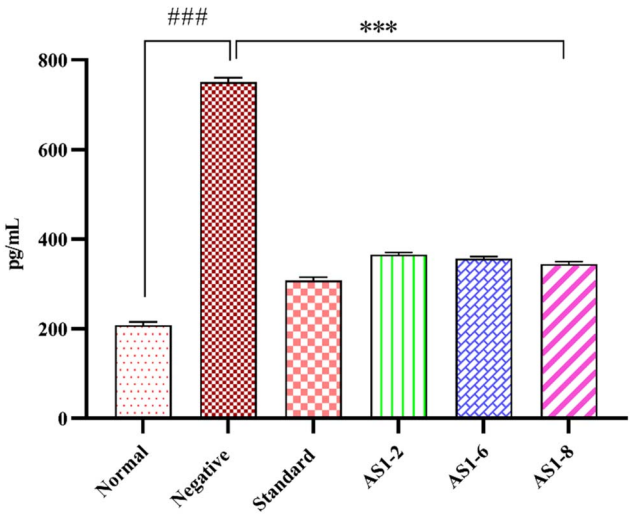

Fig. 12 Inhibitory effect of chalcone derivatives (**AS1-2**, **AS1-6**, **AS1-8**) and standard (diclofenac) against cyclooxygenase 2 (COX-2) level in carrageenan-induced paw edema model treated mice paw tissue using ELISA. $^{###}P < 0.001$ *vs.* normal. $^{***}P < 0.001$ *vs.* negative. Data are expressed as mean ± SD ($n = 3$) and analyzed using one-way ANOVA followed by the LSD comparisons test.

Additionally, the α,β-unsaturated carbonyl system in the chalcone core, known as a Michael acceptor, may contribute to the observed activity by facilitating covalent or semi-covalent interactions with nucleophilic residues in biological targets such as cysteine or lysine.[50,51] This electrophilic center is associated with irreversible inhibition in enzymes, including COX and thiol-dependent signaling proteins. The reactivity of this moiety can be modulated by the electronic nature of substituents: for example, electron-withdrawing groups (Cl, F) may increase electrophilic character and promote selective covalent interactions, while lipophilic groups like benzyl may favor non-covalent binding through π–π stacking or hydrophobic interactions.[52] These structural features may explain the differential potency observed *in vivo*. Future investigations, such as covalent docking simulations or thiol-reactivity assays (*e.g.*, glutathione trapping) are warranted to clarify the contribution of covalent binding to both efficacy and selectivity.[53]

The *in vitro* enzyme inhibition results further support the *in vivo* anti-inflammatory profile of the chalcone derivatives.

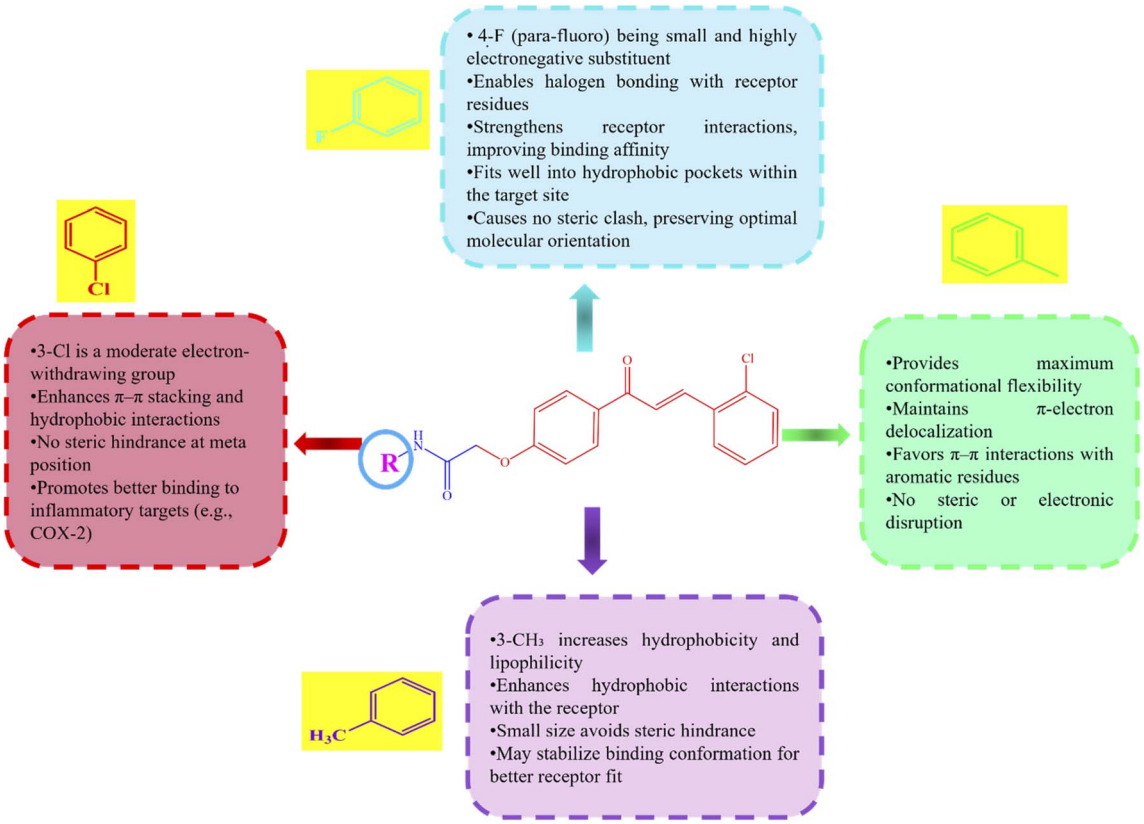

Fig. 13 Structure–activity relationship (SAR) of newly synthesized chalcone derivatives.

Notably, halogen-substituted derivatives **AS1-2** (3–Cl–Ph) and **AS1-6** (4–F–Ph) exhibited potent COX-2 inhibition ($IC_{50} = 3.2$ μM and 2.7 μM, respectively) with high selectivity indices (3.7 and 4.7), surpassing that of diclofenac (SI = 1.6) and comparable to the selective COX-2 inhibitor nimesulide (SI = 3.8). The benzyl derivative **AS1-8** also showed significant COX-2 inhibition ($IC_{50} =$ 4.1 μM; SI = 3.7), consistent with its strong activity in the carrageenan-induced paw edema model. These findings suggest that electron-withdrawing halogens enhance the electrophilic nature of the chalcone enone system, favoring interactions within the COX-2 active site.[49] While lipophilic benzyl groups may stabilize binding *via* hydrophobic contacts. Importantly, *ex vivo* ELISA results from carrageenan-induced paw tissue confirmed a reduction in COX-2 protein levels upon treatment with **AS1-2**, **AS1-6**, and **AS1-8**, aligning with their enzyme-based inhibitory profiles. Together, these data reinforce that substitution with halogens or bulky lipophilic groups at the amide-linked aryl moiety modulates selectivity toward COX-2, a desirable feature for minimizing gastrointestinal side effects associated with non-selective COX inhibition. While chalcones are a well-explored scaffold in anti-inflammatory research, the design strategy employed in this study focused on the rational incorporation of amide-linked aryl substitutions to modulate physicochemical and biological properties. The novelty of this series lies in the specific combination of an electron-rich or electron-deficient aryl amide moiety with a fixed chalcone backbone, aiming to enhance COX-inhibition, bioavailability, and reduce off-target toxicity. Recent literature suggests that fine-tuning the amide region of chalcones can drastically affect selectivity and metabolic stability.[54] Although substitutions were confined to the amide side, they represent electronically and sterically diverse functionalities (halogen, methyl, benzyl), allowing initial exploration of pharmacophoric requirements. The small compound set limits broad SAR extrapolation, but the results provide a focused structure-guided pilot dataset to inform future optimization at both amide and chalcone regions. Expanding substitution on the enone and aryl ketone regions in future libraries will be essential to gain deeper SAR insights and increase scaffold novelty.

3 Materials and methods

3.1 Chemicals and instruments

All experiments were conducted under normal atmospheric conditions. Analytical grade solvents and chemicals, along with 4-hydroxyacetophenone, 2-chlorobenzaldehydes, and different anilines and amines from Sigma-Aldrich, were used as received. The progress of the reactions was monitored by thin-layer chromatography (TLC) using Merck silica gel plates, and visualization was achieved under UV light. The compounds' purity was confirmed by recrystallization from methanol. Proton nuclear magnetic resonance (^{1}H-NMR) and carbon nuclear magnetic resonance (^{13}C-NMR) spectra were acquired on a Bruker AV-300 spectrometer operating at 300 MHz and 75 MHz, respectively, with deuterated chloroform ($CDCl_3$) as the solvent and

tetramethylsilane (TMS) as the internal reference. Mass spectra were obtained using electron impact mass spectrometry (EIMS) on a JEOL JMS 600H-1 instrument. Fourier-transform infrared (FTIR) spectra were recorded on a Bruker Alpha FTIR spectrophotometer (OPUS-7.5.18). Melting points were determined using a Gallenkamp SAYO MPD BM 3.5 apparatus.

3.2 Synthesis of the chalcone derivatives

The targeted chalcone derivatives were synthesized in three steps, as shown below.

3.2.1 General protocol for the synthesis of chalcone through Claisen–Schmidt condensation reaction (3, step 1). In a round-bottom flask placed in an ice bath, 4-hydroxyacetophenone (0.01 mol) and 2-chlorobenzaldehyde (0.01 mol) were dissolved in methanol (40 mL). After stirring for 30 min, 60% NaOH solution (10 mL) was added dropwise. The resulting viscous mixture was stirred at room temperature for 2–3 h, left to stand overnight under cooling conditions, then diluted with 40 mL of ice-cold distilled water, filtered, washed, air-dried, and finally recrystallized from ethanol.[55]

3.2.2 General protocol for the synthesis of 2-chloro-*N*-arylacetamides (VIa-*k*, step 2). After substituted anilines and amines (1.9 mmol) were dissolved in dichloromethane (DCM) along with triethylamine (2.18 mmol), 2-chloroacetyl chloride was added dropwise (2.09 mmol) while keeping the temperature between 0 and 5 °C. TLC was used to track the reaction mixture's progress over a one-hour stirring period. Precipitation of the resultant product occurred on ice, filtered, air-dried, and purified by recrystallization from methanol.[56]

3.2.3 General synthetic procedure for chalcone derivatives (AS1-1–AS1-11, step 3). Potassium iodide (3 mmol) was used to stir a combination of 4-hydroxy chalcone (0.589 mmol), anhydrous potassium carbonate (3 mmol), and 2-chloro-*N*-arylacetamides (**6a–k**) (0.589 mmol) in dry DMF for 8 h at 50 °C. TLC tracked the course of the reaction. The final step was to add the mixture to crushed ice, filter, air dry, and recrystallize the precipitated products (**AS1-1–AS1-11**) using methanol.[57]

The synthesized chalcone derivatives (**AS1-1–AS1-11**) were characterized using spectroscopic techniques, and their hydrogen and carbon atoms were well-positioned for optimal ^{1}H-NMR and ^{13}C-NMR analyses, as illustrated in Fig. 14.

*3.2.3.1 (E)-N-(4′-Chlorophenyl)-2-(4″-(3‴-(2⁗-chlorophenyl) acryloyl)phenoxy)acetamide (**AS1-1**).* Yield: 87% (light yellow powder); m.p.:182–184 °C; R_f 0.72 (chloroform : acetone; 9 : 1); FTIR (ATR, $\bar{\upsilon}$,cm^{-1}) 3408 (N–H stretch), 3198 (Csp^2-H, aromatic), 3132 (Csp^3-H, aliphatic), 1685 (C=O stretch, ketone), 1650 (C=O stretch, amide), 1590 (C=C aromatic), 1545 (C=C α,β-unsaturated), 749 (C–Cl); ^{1}H-NMR (300 MHz, $CDCl_3$): δ (ppm) 8.27 (1H, s, N–H), 8.19 (1H, d, ^{3}J = 15.9 Hz, H-3‴), 8.11–8.07 (2H, m, H-3″, 5″), 7.78–7.74 (1H, m, H-6⁗), 7.60–7.55 (2H, m, H-2′, 6′), 7.60–7.31 (8H, m, H-2″, 2‴, 6″, 3′, 5′, 3⁗, 4⁗, 5⁗), 4.71 (2H, s, H-2); ^{13}C-NMR (75 MHz, $CDCl_3$): δ (ppm) 188.60 (C-1‴), 165.41 (C-1), 160.37 (C-1″), 140.51 (C-3‴), 135.21 (C-1⁗), 135.49 (C-1′), 133.23 (C-2⁗), 132.51 (C-4″), 131.22 (C-3″, 5″), 130.35–127.11 (C-3⁗, 4⁗, 5⁗, 6⁗), 130.16 (C-4′), 129.20 (C-3′, 5′), 124.38 (C-2‴), 121.45 (C-2′, 6′), 114.70 (C-2″), 67.40 (C-2); EIMS *m*/*z* (%); 425.2 (100, M$^+$), 390.1 (69.2), 271.2 (13.1), 243.0 (11.0), 223.1 (28.2), 194 (4.5), 184.2 (23.0), 168.0 (3.9), 166.0 (4.9), 156.1 (13.6), 137.0 (7.5), 126.1 (5.5), 102.5 73.1), 91.1 (27.1), 77.0 (19.4), 65.0 (5.2), 43.0 (4.2).

*3.2.3.2 (E)-N-(3′-Chlorophenyl)-2-(4″-(3‴-(2⁗-chlorophenyl) acryloyl)phenoxy)acetamide (**AS1-2**).* Yield: 84% (yellow powder); m.p. :176–178 °C; R_f 0.68 (chloroform : acetone; 9 : 1); FTIR (ATR, $\bar{\upsilon}$,cm^{-1}) 3401 (N–H ′ stretch), 3196 (Csp^2-H, aromatic), 3136 (Csp^3-H, aliphatic), 1694 (C=O stretch, ketone), 1654 (C=O stretch, amide), 1593 (C=C aromatic), 1526 (C=C α,β-unsaturated), 753 (C–Cl); ^{1}H-NMR (300 MHz, $CDCl_3$): δ (ppm) 8.29 (1H, s, N–H), 8.11–8.08 (2H, m, H-3″, 5″), 8.10 (1H, d, ^{3}J = 15.9 Hz, H-3‴), 7.78–7.08 (12H, m, H-2′, 3′, 4′, 5′, 6′, 2″, 6″, 2‴, 3⁗, 4⁗, 5⁗, 6⁗), 4.71 (2H, s, H-2); ^{13}C-NMR (75 MHz, $CDCl_3$): δ (ppm) 188.62 (C-1‴), 165.50 (C-1), 160.35 (C-1″), 140.51 (C-3‴), 137.76 (C-1′), 135.49 (C-3′), 134.82 (C-1⁗), 133.23 (C-2⁗), 130.35 (C-4″), 131.22 (C-3″, 5″), 132.52–125.16 (C-4′, 5′, 3⁗, 4⁗, 5⁗, 6⁗), 124.38 (C-2‴), 120.29 (C-2′), 118.14 (C-6′), 114.71 (C-2″, 6″), 67.40 (C-2); EIMS: *m*/*z* (%); 425.2 (100, M$^{\cdot+}$), 390.1 (80.2), 271.2 (15.1), 243.0 (9.0), 223.1 (30.0), 194 (4.5), 184.2 (27.0), 168.0 (3.19), 166.0 (4.9), 156.1 (13.6), 137.0 (9.5), 126.1 (2.5), 102.5 (3.1), 91.1 (17.1), 77.0 (12.4), 65.0 (5.2), 43.0 (7.2).

*3.2.3.3 (E)-N-(4′-Bromophenyl)-2-(4″-(3‴-(2⁗-chlorophenyl) acryloyl)phenoxy)acetamide (**AS1-3**).* Yield: 82% (yellow powder); m.p. :166–168 °C; R_f 0.68 (chloroform : acetone; 9 : 1); FTIR (ATR, $\bar{\upsilon}$,cm^{-1}) 3409 (N–H stretch), 3196 (Csp^2-H, aromatic), 3136 (Csp^3-H, aliphatic), 1687 (C=O stretch, ketone), 1653 (C=O stretch, amide), 1594 (C=C, aromatic), 1516 (C=C α,β-unsaturated), 751 (C–Cl); ^{1}H-NMR (300 MHz, $CDCl_3$): δ (ppm) 8.26 (1H, s, N–H), 8.19 (1H, d, ^{3}J = 15.9 Hz, H-3‴), 8.12–8.08 (2H, m, H-3″, 5″), 7.78–7.74 (1H, m, H-6⁗), 7.55–7.33 (8H, m, H-2′, 3′, 5′, 6′, 2‴, 3⁗, 4⁗, 5⁗), 7.12–7.08 (2H, m, H-2″, 6″), 4.70 (2H, s, H-2); ^{13}C-NMR (75 MHz, $CDCl_3$): δ (ppm) 188.59 (C-1‴), 165.40(C-1), 160.36 (C-1″), 140.51 (C-3‴), 135.73 (C-1′), 135.49 (C-2⁗), 133.24 (C-1⁗), 132.53 (C-3⁗), 132.53–127.11 (4C, C-3⁗, 4⁗, 5⁗, 6⁗), 132.16 (C-3″, 5″), 130.35 (C-4″), 131.22 (C-3′, 5′), 124.39 (C-2‴), 121.74 (C-2′, 6′), 117.80 (C-4′), 114.71 (C-2″, 6″), 67.42 (C-2); EIMS *m*/*z* (%); 469.0 (100, M$^{\cdot+}$), 434.0 (80.2), 271.2 (15.1), 243.0 (9.0), 228.0 (11.0), 212.0 (19.0), 200.0 (3.5), 223.1 (30.0), 194 (4.5), 170.0 (22.3) 166.0 (4.9), 137.0 (9.5), 102.5 (3.1), 91.1 (14.1), 77.0 (12.4), 65.0 (3.8), 43.0 (11.2).

*3.2.3.4 (E)-N-(4′-Nitrophenyl)-2-(4″-(3‴-(2⁗chlorophenyl) acryloyl)phenoxy)acetamide (**AS1-4**).* Yield: 67% (dark brown powder); m.p. :155–157 °C; R_f 0.65 (chloroform : acetone; 9 : 1);

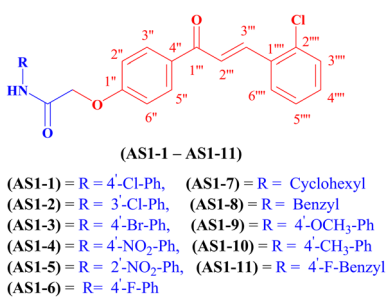

(AS1-1 – AS1-11)

(AS1-1) = R = 4′-Cl-Ph, (AS1-7) = R = Cyclohexyl
(AS1-2) = R = 3′-Cl-Ph, (AS1-8) = R = Benzyl
(AS1-3) = R = 4′-Br-Ph, (AS1-9) = R = 4′-OCH_3-Ph
(AS1-4) = R = 4′-NO_2-Ph, (AS1-10) = R = 4′-CH_3-Ph
(AS1-5) = R = 2′-NO_2-Ph, (AS1-11) = R = 4′-F-Benzyl
(AS1-6) = R = 4′-F-Ph

Fig. 14 Chemical structure of the newly synthesized chalcone derivatives (AS1-1–AS1-11), highlighting the core chalcone framework with variable substituents (*R*) at the designated position.

FTIR (ATR, $\bar{\nu}$,cm^{-1}) 3320 (N–H stretch), 3198 (Csp^2-H, aromatic), 2920 (Csp^3-H, aliphatic), 1653 (C=O stretch, ketone), 1588 (C=O stretch, amide), 1501 (C=C aromatic), 1436 (C=C α,β-unsaturated),745 (C–Cl); ^{1}H-NMR (300 MHz, CDCl$_3$): δ (ppm) 8.28–8.03 (5H, m, H-3′, 5′, 3‴, 3″, 5″), 7.80–7.32 (4H, m, N–H, 2′, 6′, 6⁗), 7.29–6.99 (6H, m, H-2″, 6″, 2‴, 3⁗, 4⁗, 5⁗), 4.75 (2H, s, H-2); ^{13}C-NMR (75 MHz, CDCl$_3$): δ (ppm) 188.57 (C-1‴), 167.28 (C-1), 160.70 (C-1″), 140.37 (C-4′), 137.57 (C-1′), 135.47 (C-3‴), 133.30 (C-2⁗), 132.14 (C-1⁗), 131.12 (C-3″, 5″), 130.33 (C-4″), 128.83–124.47 (10C, C-2′, 6′, 3⁗, 4⁗, 5⁗, 6⁗, 2‴,3′, 5′), 114.60 (C-2″, 6″), 67.31 (C-2); EIMS *m*/*z* (%); 436.1 (100, M$^{\cdot+}$), 401.1 (50.2), 271.2 (22.1), 243.0 (11.0), 223.1 (17.0), 195.1 (43.5), 194 (14.5), 179.1 (13.3), 167.1 (7.5), 166.0 (11.9), 137.1 (16.8), 137.0 (26.5), 102.5 (3.1), 91.0 (19.0), 77.0 (20.4), 65.0 (53.3), 43.0 (2.2).

*3.2.3.5 (E)-N-(2′-Nitrophenyl)-2-(4″-(3‴-(2⁗-chlorophenyl) acryloyl)phenoxy)acetamide (**AS1-5**).* Yield: 71% (off white powder); m.p. :185–187 °C; R_f 0.78 (chloroform : acetone; 9 : 1); FTIR (ATR, $\bar{\nu}$,cm^{-1}) 3290 (N–H stretch), 3198 (Csp^2-H, aromatic), 2920 (Csp^3-H, aliphatic), 1703 (C=O stretch, ketone), 1650 (C=O stretch, amide), 1592 (C=C aromatic), 1553 (C=C α,β-unsaturated), 744 (C–Cl); ^{1}H-NMR (300 MHz, CDCl$_3$): δ (ppm) 11.65 (1H, s, N–H), 8.91 (1H, dd, ^3J = 8.4 Hz, ^4J = 1.8 Hz, H-3′), 8.29 (1H, dd, ^3J = 8.4 Hz, ^4J = 1.8 Hz, H-3′), 8.19 (1H, d, ^3J = 15.6 Hz, H-3‴), 8.13–8.08 (2H, m, H-3″, 5″), 7.78–7.24 (7H, m, H-4′, 5′, 2‴, 3⁗, 4⁗, 5⁗, 6⁗), 7.20–716 (2H, m, H-2″, 6″), 4.77 (2H, s, H-2); ^{13}C-NMR (75 MHz, CDCl$_3$): δ (ppm) 188.61 (C-1‴), 166.65 (C-1), 160.32 (C-1″), 140.38 (C-3‴), 136.51 (C-2′), 136.16 (C-1′), 135.49 (C-4′), 131.20 (C-3″, 5″), 133.80–124.02 (8C, C-5′, 6′, 1⁗, 2⁗, 3⁗, 4⁗, 5⁗), 130.21 (C-4″), 124.44 (C-2‴), 121.19 (C-3′), 67.29 (C-2); EIMS *m*/*z* (%); 436.1 (100, M$^{\cdot+}$), 401.1 (55.2), 271.2 (25.1), 243.0 (15.0), 223.1 (12.0), 195.1 (33.5), 194 (14.5), 179.1 (13.3), 167.1 (7.3), 166.0 (16.1), 137.1 (11.8), 137.0 (29.5), 102.5 (13.1), 91.0 (16.9), 77.0 (15.4), 65.0 (53.3), 43.0 (2.6).

*3.2.3.6 (E)-N-(4′-Fluorophenyl)-2-(4″-(3‴-(2⁗-chlorophenyl) acryloyl)phenoxy)acetamide (**AS1-6**).* Yield: 83% (light brown powder); m.p. :172–174 °C; R_f 0.73 (chloroform : acetone; 9 : 1); FTIR (ATR, $\bar{\nu}$,cm^{-1}) 3410 (N–H stretch), 3190 (Csp^2-H, aromatic), 2920 (Csp^3-H, aliphatic), 1684 (C=O stretch, ketone), 1652 (C=O stretch, amide), 1594 (C=C aromatic), 1561 (C=C α,β-unsaturated), 753 (C–Cl); ^{1}H-NMR (300 MHz, CDCl$_3$): δ (ppm) 8.25 (1H, s, N–H), 8.12–8.07 (2H, m, H-3″, 5″), 8.10 (1H, d, ^3J = 15.9 Hz, H-3‴), 7.78–7.74 (1H, m, H-6⁗), 7.60–7.55 (2H, m, H-3′, 5′), 7.48–7.31 (4H, m, H-2‴, 3⁗, 4⁗, 5⁗), 7.13–7.04 (4H, m, H-2′, 6′, 2″, 6″), 4.71 (1H, s, H-2); ^{13}C-NMR (75 MHz, CDCl$_3$): δ (ppm) 188.61 (C-1‴), 165.39 (C-1), 160.44 (C-1″), 155.49 (C-4′), 140.50 (C-3‴), 135.49 (C-1′) 133.24 (C-2⁗), 132.47 (C-1⁗), 131.22 (C-3″, 5″), 130.35 (C-4″), 127.79–116.02 (C-3⁗, 4⁗, 5⁗, 6⁗), 124.39 (C-2‴), 122.10 (C-2′, C-4′), 115.72 (C-3′ C-5′), 114.70 (C-2″, 6″); EIMS *m*/*z* (%); 409.1 (100, M$^{\cdot+}$), 374.1 (50.2), 271.2 (22.1), 243.0 (11.0), 228.0 (13.0), 223.1 (17.0), 194 (4.5), 168.0 (29.3) 166.0 (1.9), 152.1 (5.4), 137.0 (26.5), 124.1 (1.0), 102.5 (11.1), 91.0 (16.1), 77.0 (12.4), 65.0 (3.3), 43.0 (6.2).

*3.2.3.7 (E)-N-(Cyclohexyl)-2-(4″-(3‴-(2⁗-chlorophenyl) acryloyl)phenoxy)acetamide (**AS1-7**).* Yield: 74% (off white powder); m.p. :146–148 °C; R_f 0.65 (chloroform : acetone; 9 : 1); FTIR (ATR, $\bar{\nu}$,cm^{-1}) 3276 (N–H stretch), 3190 (Csp^2-H, aromatic), 2920 (Csp^3-H, aliphatic), 1653 (C=O stretch, ketone), 1598 (C=O stretch, amide), 1550 (C=C aromatic), 1505 (C=C α,β-unsaturated), 753 (C–Cl); ^{1}H-NMR (300 MHz, CDCl$_3$): δ (ppm) 8.18 (1H, d, ^3J = 15.9 Hz, H-3‴), 8.09–8.04 (2H, m, H-3″, 5″), 7.78–7.75 (1H, m, H-6⁗), 7.52–7.32 (4H, m, H-2‴, 3⁗, 4⁗, 5⁗), 7.06–7.01 (2H, m, H-2″, 6″), 6.38 (1H, d, ^3J = 7.2 Hz, N–H), 3.96–3.83 (1H, m, H-1′), 1.98–1.19 (10H, m, H-2′, 3′, 4′, 5′, 6′); ^{13}C-NMR (75 MHz, CDCl$_3$): δ (ppm) 188.61 (C-1‴), 166.31 (C-1), 160.82 (C-1″), 141.32 (C-3‴), 135.40 (C-1⁗), 133.32 (C-2⁗), 132.12 (C-4″), 131.11 (C-3″, 5″), 130.33–127.08 (4C, C-3⁗, 4⁗, 5⁗, 6⁗), 124.51 (C-2‴), 114.62 (C-2″, 6″), 67.38 (C-2), 48.01 (C-1′), 33.00 (C-2′, 6′), 25.42 (C-3′, C-5′), 24.79 (C-4′); EIMS *m*/*z* (%); 405.1 (100, M$^{\cdot+}$), 369.1 (49.2), 271.2 (22.1), 243.0 (10.0), 223.1 (12.0), 194 (9.5), 156.1 (23.3), 137.0 (26.5), 126.1 (7.0), 102.5 (13.1), 91.0 (13.1), 77.0 (2.4), 65.0 (1.9), 43.0 (1.0).

*3.2.3.8 (E)-N-(Benzyl)-2-(4″-(3‴-(2⁗-chlorophenyl)acryloyl) phenoxy)acetamide (**AS1-8**).* Yield: 79% (off white powder); m.p. :168–170 °C; R_f 0.61 (chloroform : acetone; 9 : 1); FTIR (ATR, $\bar{\nu}$,cm^{-1}) 3277 (N–H stretch), 3190 (Csp^2-H, aromatic), 2920 (Csp^3-H, aliphatic), 1658 (C=O stretch, ketone), 1601 (C=O stretch, amide), 1544 (C=C aromatic), 1502 (C=C α,β-unsaturated), 737 (C–Cl); ^{1}H-NMR (300 MHz, CDCl$_3$): δ (ppm) 8.18 (1H, d, ^3J = 15.9 Hz, H-3‴), 8.08–8.03 (2H, m, H-3″, 5″), 7.51–7.29 (9H, m, H-2′, 3′, 4′, 5′, 6′, 2‴, 3⁗, 4⁗, 5⁗), 7.77–7.74 (1H, m, H-6⁗), 7.05–7.00 (2H, m, H-2″, 6″), 6.89 (1H, t, ^3J = 4.2 Hz, N–H), 4.65 (2H, s, H-2), 4.58 (2H, d, ^3J = 6.6 Hz, (Benzylic CH$_2$); ^{13}C-NMR (75 MHz, CDCl$_3$): δ (ppm) 188.57 (C-1‴), 167.28 (C-1), 160.70 (C-1″), 140.39 (C-3‴), 137.57 (C-1′), 135.47 (C-1⁗), 133.30–127.09 (10C, C-2, 3, 4, 5, 6, 2‴, 3⁗, 4⁗, 5⁗, 6⁗), 131.14 (C-3″, 5″), 114.60 (C-2″, 6″), 67.31 (C-2), 43.11 (Benzylic CH$_2$); EIMS *m*/*z* (%); 405.1 (100, M$^{\cdot+}$), 369.6 (45.2), 271.2 (17.1), 243.0 (7.0), 223.1 (17.0), 194 (4.5), 164.1 (4.3) 166.0 (3.9), 148.1 (11.4), 137.0 (11.5), 104.1 (9.0), 102.5 (2.1), 91.1 (11.6), 77.0 (4.4), 65.0 (2.3), 43.0 (1.2).

*3.2.3.9 (E)-N-(4′-Methoxyphenyl)-2-(4″-(3‴-(2⁗-chlorophenyl)acryloyl)phenoxy) acetamide (**AS1-9**).* Yield: 81% (light brown powder); m.p. :135–137 °C; R_f 0.71 (chloroform : acetone; 9 : 1); FTIR (ATR, $\bar{\nu}$,cm^{-1}) 3394 (N–H stretch), 3073 (Csp^2-H, aromatic), 3012 (Csp^3-H, aliphatic), 1658 (C=O stretch, ketone), 1597 (C=O stretch, amide), 1535 (C=C aromatic), 1504 (C=C α,β-unsaturated), 747 (C–Cl); ^{1}H-NMR (300 MHz, CDCl$_3$): δ (ppm) 8.20 (1H, d, ^3J = 15.9 Hz, H-3‴), 8.18 (1H, s, N–H), 8.11–8.08 (2H, m, H-3″, 5″), 7.78–7.33 (5H, m, H-2′,6′, 3⁗, 4⁗, 5⁗, 6⁗), 7.12–7.09 (2H, m, H-2″, 6″), 6.93–6.89 (3H, m, H-3′, 5′), 4.71 (1H, s, H-2), 3.81 (3H, s, *p*-OCH$_3$); ^{13}C-NMR (75 MHz, CDCl$_3$): δ (ppm) 188.66 (C-1‴), 165.28 (C-1), 160.56 (C-1″), 140.48 (C-3‴), 133.26–122.11 (C-1′, 4′, 4″, 2⁗, 3⁗, 4⁗, 5⁗, 6⁗), 131.22 (C-3″, 5″), 124.41 (C-2‴), 122.20 (C-2′, 6′), 114.73 (C-2″, 6″), 67.43 (C-2), 55.51 (*p*-OCH$_3$); EIMS *m*/*z* (%); 421.2 (100, M$^{\cdot+}$), 386.1 (50.2), 271.2 (22.1), 243.0 (11.0), 223.1 (17.0), 194 (4.5), 180.0 (8.3) 166.0 (23.9), 152.0 (9.4), 137.0 (26.5), 122.1 (8.0), 102.5 (2.1), 91.0 (12.1), 77.0 (10.4), 65.0 (1.3), 43.0 (6.2).

*3.2.3.10 (E)-N-(4′-Methylphenyl)-2-(4″-(3‴-(2⁗-chlorophenyl) acryloyl)phenoxy) acetamide (**AS1-10**).* Yield: 90% (light yellow powder); m.p. :167–169 °C; R_f 0.68 (chloroform : acetone; 9 : 1); FTIR (ATR, $\bar{\nu}$,cm^{-1}) 3395 (N–H stretch), 3073 (Csp^2-H, aromatic), 3012 (Csp^3-H, aliphatic), 1657 (C=O stretch, ketone), 1598 (C=O stretch, amide), 1534 (C=C aromatic), 1509 (C=C α,β-unsaturated), 755 (C–Cl); ^{1}H-NMR (300 MHz, CDCl$_3$): δ (ppm)

8.19 (1H, s, N–H), 8.16 (1H, d, $^3J = 15.9$ Hz, H-3‴), 7.78–7.33 (7H, m, H-2‴, 3′, 5′, 3⁗, 4⁗, 5⁗, 6⁗), 7.18 (1H, d, $^3J = 8.1$ Hz, H-2′, 6′), 7.13 (1H, d, $^3J = 8.7$ Hz, H-2″, 6″), 4.70 (1H, s, H-2), 2.35 (3H, s, *p*-CH_3); ^{13}C-NMR (75 MHz, $CDCl_3$): δ (ppm) 188.61 (C-1‴), 165.25 (C-1), 160.54 (C-1″), 140.43 (C-3‴), 135.49–127.10 (C-1′, 3′, 4′, 5′, 1″, 3″, 4″, 5″, 1⁗, 2⁗, 3⁗, 4⁗, 5⁗, 6⁗), 124.43 (C-2‴), 120.31 (C-2′, 6′), 114.72 (C-2″, 6″), 67.47 (C-2), 20.94 (*p*-CH_3); EIMS *m*/*z* (%); 405.1 (100, $M^{\cdot+}$), 370.2 (86.2), 271.2 (25.1), 243.0 (9.0), 223.1 (30.0), 194 (4.5), 166.0 (4.9), 164.9 (16.6), 148.2 (15.4), 137.0 (9.5), 136.1 (1.5), 106.0 (21.9) 102.5 (3.1), 91.1 (14.1), 77.0 (11.4), 65.0 (5.8), 43.0 (9.2).

*3.2.3.11 (E)-N-(4′-Fluorobenzyl)-2-(4″-(3‴-(2⁗-chlorophenyl) acryloyl)phenoxy) acetamide (**AS1-11**).* Yield: 80% (brown powder); m.p. :136–138 °C; R_f 0.67 (chloroform : acetone; 9 : 1); FTIR (ATR, $\bar{\nu}$,cm^{-1}) 3307 (N–H stretch), 3070 (Csp^2-H, aromatic), 3012 (Csp^3-H, aliphatic), 1645 (C=O stretch, ketone), 1596 (C=O stretch, amide), 1548 (C=C aromatic), 1505 (C=C α,β-unsaturated), 751 (C–Cl); ^{1}H-NMR (300 MHz, $CDCl_3$): δ (ppm) 8.24 (1H, d, $^3J = 15.9$ Hz, H-3‴), 8.08–8.03 (2H, m, H-3″, 5″), 7.77–7.01 (11H, m, H-2′, 3′, 5′, 6′, 2″, 6″, 2‴, 3⁗, 4⁗, 5⁗, 6⁗), 6.90 (1H, t, $^3J = 5.4$ Hz, N–H), 4.64 (2H, s, H-2), 4.54 (2H, d, $^3J = 6.0$ Hz, Benzylic CH_2); ^{13}C-NMR (75 MHz, $CDCl_3$): δ (ppm) 188.60 (C-1‴), 167.39 (C-1), 163.93 (C-4′), 160.63 (C-1″), 140.42 (C-3‴), 135.48 (C-1′), 133.42 (C-1⁗), 133.38 (C-2⁗), 133.26 (C-3″, 5″), 132.21–127.10 (7C, C-2′, 6′, 4″, 3⁗, 4⁗, 5⁗, 6⁗), 124.41 (C-2‴), 115.69 (d, $^2J = 21$ Hz, C-3′, 5′), 114.58 (C-2″, 6″), 67.24 (C-2), 42.39 (Benzylic CH_2); EIMS *m*/*z* (%); 423.1 (100, $M^{\cdot+}$), 387.5 (40.2), 271.2 (22.1), 243.0 (11.0), 223.1 (17.0), 194 (4.5), 180.2 (9.3), 166.1 (5.1), 166.0 (8.9), 152.1 (7.4), 137.0 (26.5), 122.1 (8.0), 102.5 (2.1), 91.0 (12.1), 77.0 (10.4), 65.0 (1.3), 43.0 (6.2).

4 *In vitro* toxicity analysis

4.1 Hemolytic assay

A hemolysis assay was conducted to evaluate the interaction of the test samples with human erythrocytes, following a standard protocol.[58] Fresh human blood was collected in EDTA tubes to prevent coagulation, washed with PBS, and adjusted to a 5% cell suspension. Aliquots of 150 μL of each sample were mixed with 350 μL of the erythrocyte suspension and incubated at 37 °C for 30 min, followed by centrifugation. Subsequently, 200 μL of the supernatant was transferred to a 96-well plate, and absorbance was recorded at 530 nm to calculate the percentage hemolysis.

$$\%\ \text{Hemolysis} = \frac{(A_s - A_n)}{(A_p - A_n)} \times 100$$

where A_s is the sample absorbance; A_n is the absorbance of the negative control; A_p is the absorbance of the positive control.

4.2 Brine shrimp lethality assay

In a 96-well microplate, the brine shrimp lethality test was carried out following the protocol described in[59] with slight modifications. At 30 to 32 °C, *Artemia salina* eggs were incubated in simulated seawater, and the resulting nauplii were harvested using a Pasteur pipette. DMSO (<1%) was used as the solvent, and ten larvae were placed in each well containing successive dilutions of the test compounds (80, 40, 20, and 10 μg mL^{-1}). The negative and positive controls were DMSO and doxorubicin (4 mg mL^{-1} DMSO), respectively. Mortality was noted after a day, and each experiment was performed in triplicate. The LD_{50} values for all chalcone derivatives were determined using a standard brine shrimp lethality assay followed by dose–response analysis. Each compound was tested at 10, 20, 40, 80, and 200 μg mL^{-1}, and mortality was recorded after 24 hours. Percent mortality was calculated for each concentration, and when applicable, corrected using Abbott's formula. LD_{50} values were estimated by plotting log-transformed concentrations against probit-transformed mortality and performing probit regression using GraphPad Prism. Because none of the tested chalcone derivatives produced ≥50% mortality at the highest concentration evaluated (200 μg mL^{-1}), their LD_{50} values were calculated to be above this level; therefore, they are reported as $LD_{50} > 200$ μg mL^{-1}.

4.3 Cytotoxicity assay (MTT assay)

3T3 fibroblast cells were purchased from Sigma-Aldrich (product no. 90020107), and all experiments were conducted at the H.E.J. Research Institute of Chemistry, University of Karachi, Karachi-75270, Pakistan. The cells were cultured and maintained under standard conditions recommended by the supplier.

The cytotoxic potential of chalcone derivatives (**AS1-1–AS1-11**) was assessed in 3T3 fibroblast cells using the MTT assay, as originally described by Mosmann[60] and later modified by Masaud *et al.*[61] Cells were cultured in Dulbecco's Modified Eagle Medium (DMEM) supplemented with 10% fetal bovine serum (FBS) and 1% penicillin–streptomycin. For adhesion, 1×10^4 cells/well were seeded into 96-well plates and incubated overnight at 37 °C in a humidified 5% CO_2 atmosphere. The following day, 100 μL of fresh medium containing varying concentrations of test compounds was added, with doxorubicin (30 μM) as the positive control and DMSO (≤0.5% v/v) as the vehicle control. After 24–48 h of incubation, 10 μL of MTT solution (5 mg mL^{-1} in PBS) was added to each well and plates were incubated at 37 °C for 3–4 h in the dark. The medium was then removed, and 100 μL of DMSO was added to solubilize the formazan crystals. Absorbance was recorded at 570 nm with a reference wavelength of 630 nm using a microplate reader, and cell viability (%) was calculated according to the standard formula.

$$\text{Cell viability (\%)} = (\text{treatment cell absorbance}/\text{control cell absorbance}) \times 100$$

4.4 *In vitro* cyclooxygenase isoenzymes (COX-1 and COX-2) inhibitory assay

Chalcone derivatives (**AS1-1–AS1-11**) were evaluated for their inhibitory activity against COX isoenzymes (COX-1 and COX-2) under the previously established procedure.[62,63] Briefly, the enzyme was activated by mixing 50 μL of cofactor buffer (0.1 M Tris, pH 8.0, with 1 mM haematin, 0.24 mM TMPD, and 0.9 mM

glutathione) and 10 μL of enzyme solution. The mixture was subsequently kept on ice (4 °C, 5 min). Then 20 μL of test compounds (0.1–100 μM) was added into each well following 60 μL of activated enzyme–cofactor mixture. The reactions were initiated with 20 μL of arachidonic acid (30 mM), giving a total of 100 μL, after pre-incubation (5–10 min, room temperature). A microplate reader was utilized to detect absorbance at 570 nm after incubation for 15 minutes at 37 °C. Control inhibitors for COX-1 and COX-2 were diclofenac sodium and nimesulide, respectively, and appropriate blanks for correcting the baseline. Compared to these controls, percentage inhibition was calculated as follows:

$$\%\ \text{Inhibition} = \text{Abs test sample} - \text{Abs background}/(\text{Abs solvent blank} - \text{Abs background}) \times 100$$

4.4.1 Computation of the selectivity index (SI). The COX-2 selectivity of the synthesized derivatives was evaluated by calculating the selectivity index (SI), defined as the ratio of IC_{50} values for COX-1 to COX-2 (SI=IC_{50} COX-1/IC_{50} COX-2). A higher SI value denotes enhanced gastrointestinal safety, as it reflects preferential inhibition of COX-2 over COX-1, thereby minimizing the risk typically associated with non-selective NSAIDs.[64]

4.5 *In silico* ADMET evaluation

4.5.1 *In silico* absorption, distribution, metabolism, and excretion (ADME) assessment. The physicochemical and toxicity profiles of the synthesized lead compounds were assessed using the SwissADME and pkCSM platforms. In addition, SwissADME furnishes pharmacological predictions derived from physicochemical parameters.[65]

4.6 Molecular docking studies

Bioactive compounds' binding preferences were analyzed through molecular docking with protein structures from the RCSB Protein Data Bank. COX-1 (PDB ID: 3N8X) and COX-2 (PDB ID: 1PXX) 3D structures were retrieved from the Protein Data Bank. The structures were optimized, and water molecules were eliminated through Discovery Studio. ChemSketch was employed to draw out the chalcone derivatives, and Discovery Studio was employed to optimize them. PyRx, coupled with AutoDock Vina, was employed for molecular docking, and binding affinities were recorded. Schrödinger Maestro was employed for binding interaction analysis and the generation of 2D and 3D representations of docked ligand–protein complexes. This paper enlightens us about the molecular interactions and binding affinities of newly synthesised chalcone derivatives towards COX-1 and COX-2.

4.7 Molecular dynamics simulation

4.7.1 System preparation. The topology and coordinates for GROMACS were generated by the CHARMM-GUI solution builder[66] to generate the protein–ligand pair. The CHARMM36 force field[67,68] was employed to characterize the protein, while the CGenFF[69] was utilized to parameterise the ligand. In a 16 147-water-molecule periodic box, the system was neutralized with 46 K^+ and 45 Cl^- ions and solvated with the TIP3P water model.[70] An approximate bulk concentration of 0.155 M of KCl was achieved in this setup, which is compatible with near-physiological ionic strength.

4.7.2 Simulations. GROMACS 2023.2 (ref. 71) was employed to simulate on a local workstation featuring an NVIDIA GeForce RTX 5070 Ti GPU (CUDA 12.8). The minimization of the energy of the system was accomplished using the steepest descent algorithm until the maximum force was below 1000 kJ mol^{-1} nm^{-1}. Heavy atoms were restrained in positions in the two phases of equilibration, which were (i) an NVT ensemble (constant volume, 300 K, 500 ps) and (ii) an NPT ensemble (constant pressure, 1 bar, 500 ps). Under periodic boundary conditions, production MD was performed for 100 ns with a 2 fs time step. The Parrinello–Rahman barostat[72] and the V-rescale thermostat[73] were utilized to control the temperature and pressure. Trajectories were saved every ten seconds.

4.7.3 Trajectory analysis. Custom Python/Matplotlib scripts and GROMACS tools were utilized for post-processing. The radius of gyration (R_g), RMSD, RMSF, and hydrogen bond dynamics were calculated as structural and energetic properties.

4.7.3.1 Root mean square deviation (RMSD).

$$\mathrm{RMSD}(t) = \sqrt{\frac{1}{N}\sum_{i=1}^{N}\left|r_i(t) - r_i^{\mathrm{ref}}\right|^2}$$

where $r_i(t)$ is the position of atom i at time t, ri^{ref} is its position in the reference structure, and N is the number of backbone atoms.

4.7.3.2 Root mean square fluctuation (RMSF).

$$\mathrm{RMSF}(i) = \sqrt{\frac{1}{T}\sum_{t=1}^{T}\left|r_i(t) - \langle r\rangle_i\right|^2}$$

where (r_i) is the mean position and T is the number of frames.

4.7.3.3 Radius of gyration (R_g).

$$R_{\mathrm{g}} = \sqrt{\frac{\sum_{i=1}^{N} m_i |r_i - r_{\mathrm{COM}}|^2}{\sum_{i=1}^{N} m_i}}$$

where m_i is atom i's mass and r_{COM} is the system's center of mass.

4.7.3.4 Hydrogen bonds (H-bonds). Defined with donor–acceptor distance < 0.35 nm and 30° angle cutoff.

4.8 *In vivo* behavioral studies

4.8.1 Animals. Adult male and female albino mice aged 6–7 weeks and weighing 25–30 g were utilized in *in vivo* experiments. The mice were maintained in the Department of Pharmacy animal facility at QAU, Islamabad, following acquisition from the National Institute of Health (NIH) in Islamabad, Pakistan. They were kept in standard conditions, including

a 12/12 light/dark cycle, 22 °C temperature, and 60% humidity, and unlimited access to food and water. The QAU Bioethical Committee (BEC-FBS-QAU2024-688) approved all procedures. In line with WHO (2010) guidelines, human blood samples were collected with consent for the haemolytic assay. National Institutes of Health (NIH) in Pakistan has maintained its ethical principles regarding the use and management of animals.

4.8.2 Ethical approval. All experiments involving animals and human blood samples were conducted with the approval of the Bioethics Committee, Faculty of Biological Sciences, Quaid-i-Azam University, Islamabad, Pakistan (BEC-FBS-QAU2024-688 dated 28-2-25). Fresh blood samples were collected from healthy adult volunteers after obtaining written informed consent, in accordance with the World Health Organization (WHO, 2010) guidelines for blood collection.

4.8.3 Experimental groups. Multiple experimental sets were employed for the evaluation of pharmacological effects, to which the control group received standard saline injections. According to earlier research on the anti-inflammatory and antinociceptive activities, every newly synthesised chalcone derivative (10 mg kg^{-1}) was administered intraperitoneally (i.p.).[74,75] Diclofenac sodium (10 mg kg^{-1}, i.p.) was the standard drug for carrageenan-induced paw oedema test, formalin-induced paw licking test, and acetic acid-induced writhing test.

4.8.4 Acetic acid-induced writhing test. 30 minutes after chalcone derivatives were given to the animals, they received injections of 1% acetic acid. For 20 min, abdominal constrictions were noted as signs of pain.[76] Abdominal dragging and hind limb extension were indicators of abdominal constriction.[77]

4.8.5 Formalin-induced paw licking test. The protocol was employed from,[78] where mice pretreated with chalcone derivatives (10 mg kg^{-1}), diclofenac sodium (10 mg kg^{-1}), or a negative control (10 mL kg^{-1}) received an intraplantar injection of 20 μL of 2.5% formaldehyde solution. Biting or licking the injected paw for the period of acute phase I (0–5 min) and chronic phase II (15–45 min) was observed.

4.8.6 Carrageenan-induced paw edema test. The method, which was slightly modified from [79] consisted of administering the right hind paw with 20 μL of 1% carrageenan solution following intraperitoneal (i.p.) administration of chalcone derivatives (10 mg kg^{-1}). Vernier callipers were utilized to determine the oedema thickness of the paw at 0, 1, 2, 3, 4, and 5 hours.

4.9 *Ex vivo* anti-inflammatory assay

4.9.1 Enzyme-linked immunosorbent assay (ELISA) for COX-2. COX-2 enzyme-linked immunosorbent assay (ELISA) kit was employed in measuring the COX-2 according to the manufacturer's guidelines. The tissue samples from paws (approximately 50 mg) were homogenised at 15 000 rpm with the help of Silent Crusher M (Heidolph). The supernatant was subsequently harvested after centrifugation at 4000×*g* for 10 minutes.[80] Total protein concentration in all groups was determined using the bicinchoninic acid (BCA) method (Elabscience). The appropriate amount of protein was loaded on, and the levels of COX-2 were measured using an ELISA microplate reader (BioTek ELx808). Diclofenac was the control standard, while comparison was made with chalcone derivatives **AS1-2**, **AS1-6**, and **AS1-8**. Results were expressed as pg mL^{-1} of total protein following normalisation to total protein content.[81]

4.10 Statistical analysis

The data is represented as mean ± SD. IBM SPSS Statistics 25 was applied to analyze statistically. A one-way ANOVA was followed by multiple comparisons with the use of the LSD test. The LSD test for multiple comparisons was conducted after a one-way ANOVA. In addition, wherever suitable, a two-way ANOVA was applied to assess the interaction effects of factors.

5 Conclusions

In this study, a series of eleven novel chalcone derivatives (**AS1-1–AS1-11**) were synthesized, characterized, and assessed for their anti-inflammatory, antinociceptive, and safety profiles. All synthesized derivatives exhibited excellent biocompatibility, demonstrating non-significant hemolysis compared to the negative control, thereby indicating minimal red blood cell toxicity. Furthermore, low cytotoxicity was observed in brine shrimp lethality assays, with mortality rates below 50% even at the highest concentration (80 μg mL^{-1}) and LD_{50} values exceeding 200 μg mL^{-1}, suggesting a favorable safety profile. The *in vitro* cytotoxicity assay (MTT assay) demonstrated that the synthesized chalcone derivatives (**AS1-1–AS1-11**) were inactive against normal 3T3 fibroblast cells, indicating a favorable safety profile. The *in vitro* COX inhibition assays revealed that introduction of an acetamide substitution markedly enhanced COX-2 selectivity in the synthesized chalcones, with **AS1-6**, **AS1-2**, and **AS1-8** emerging as the most promising inhibitors. Their superior selectivity indices, particularly **AS1-6** (SI = 4.7), not only surpassed diclofenac but also compared favorably with nimesulide, highlighting their potential as safer COX-2-targeted alternatives to conventional NSAIDs. Notably, molecular docking studies revealed that **AS1-2** exhibited the highest binding affinity toward both COX-1 (−8.4 kcal mol^{-1}) and COX-2 (−9.9 kcal mol^{-1}), followed by **AS1-6** and **AS1-8**, indicating strong potential as COX-2 inhibitors. The molecular dynamics simulations confirmed that **AS1-6** remained firmly anchored within the active site throughout the 100 ns trajectory, with stable hydrophobic and hydrogen bonding interactions, supporting the overall structural compactness and persistence of the protein–ligand complex. These computational predictions were further substantiated by the carrageenan-induced paw edema model, where **AS1-2**, **AS1-6**, and **AS1-8** demonstrated substantial anti-inflammatory effects, significantly reducing paw thickness at the 5 h mark. Their efficacy was comparable to that of the standard drug, reinforcing the proposed COX-inhibitory mechanism of action. *In vivo* evaluations also revealed that compounds **AS1-10**, **AS1-6**, and **AS1-2** exhibited the most substantial antinociceptive activity in the acetic acid-induced writhing test, reducing writhing counts to values comparable to the standard drug diclofenac. Similarly, in the paw-licking test induced by formalin, these compounds significantly reduced both early and late-phase nociceptive responses.

This activity is likely attributed to structural features such as 2′-Cl (**AS1-2**), 4′-F (**AS1-6**), and 4′-CH_3 (**AS1-10**) substituents, which enhance receptor interaction and membrane permeability. Overall, the presented chalcone derivatives, particularly **AS1-2**, **AS1-6**, **AS1-8**, and **AS1-10**, emerged as promising lead compounds with potent anti-inflammatory and analgesic potential, alongside favorable biocompatibility and safety profiles. Overall, the presented chalcone derivatives, particularly **AS1-2**, **AS1-6**, **AS1-8**, and **AS1-10**, emerged as promising lead compounds with potent anti-inflammatory and analgesic potential. The chalcone derivatives (**AS1-2**, **AS1-6**, and **AS1-8**) significantly reduced COX-2 expression in ELISA, showing anti-inflammatory activity comparable to diclofenac and highlighting the role of halogen substitution and amide linkage in enhancing potency. These compounds collectively offer a favorable pharmacological and safety profile, although further optimization and in-depth pharmacokinetic and mechanistic evaluations are warranted to support future therapeutic applications. While these initial findings are encouraging, the limited compound library and early-stage evaluations warrant further structural optimization and detailed pharmacological investigations to fully establish their therapeutic potential.

Ethical statement

All experiments were approved by the Bioethics Committee at Quaid-i-Azam University, Islamabad, Pakistan (BEC-FBS-QAU-2024-688, dated 28 February 2025). All the experiments involving fresh human blood samples were performed in accordance with the Guidelines of the World Health Organization (WHO, 2010)[82] and were approved by the Bioethics Committee at Quaid-i-Azam University, Islamabad, Pakistan. All the samples were collected from healthy adult volunteers after obtaining written informed consent.

Author contributions

Conceptualisation, N. I., and K. B.; methodology, A. S., and S. M. M.; software, H. N., and K. B.; validation of study, A. S., H. N., and S. M. M.; formal analysis, H. N., M. L., I. H., and T. H.; investigation, S. M. M., K. B., and H. N.; resources, N. I., and K. B.; data curation, M. L., T. H., and S. A. R.; writing – original draft preparation, A. S., N. I., S. M. M., K. B., and M. L.; writing – review and editing, A. S., N. I., K. B., T. H., S. A. R., and M. L.; visualisation, S. A. R., N. I., K. B., T. H., and M. L.; supervision, N. I., and K. B.; project administration, N. I.; funding acquisition, T. H., S. A. R., N. I., molecular dynamics simulations, computational analyses (RMSD, RMSF, R_g, H-bond), simulation-related methods and results, I. M. All authors have reviewed and approved the final version of the manuscript for publication.

Conflicts of interest

The authors affirm that no conflicts of interest are associated with the publication of this work.

Data availability

The manuscript includes all relevant data which was generated or analyzed during this study. Additional information is included in the supplementary information (SI). Supplementary information: all the synthesised chalcone derivatives (**AS1-1**–**AS1-11**) contain spectrum characterisation data, in particular ^{13}C-NMR, ^{1}H-NMR spectras, expansions of ^{13}C-NMR, ^{1}H-NMR, FTIR, and EIMS spectra (Fig. S1–S78), in the SI. ^{19}F-NMR analyses were performed for all fluorinated chalcone derivatives, and the corresponding spectra are provided in the SI (Fig. S37 and S78). Fig. S35–S40 present the molecular docking interaction diagrams with COX-1 and COX-2. Physical information and structures for derivatives are presented in Tables S1 and S2. The predicted toxicological profiles from pkCSM (Table S8) and *in silico* ADME and drug-likeness predictions from SwissADME (Tables S3–S7) are included. See DOI: https://doi.org/10.1039/d5ra07230a.

Acknowledgements

The authors extend their appreciation to the Deanship of Scientific Research, King Saud University, for funding through the Vice Deanship of Scientific Research Chairs, Research Chair for Biomedical Applications of Nanomaterials. For the arrangement of the needed research equipment, the authors extend their gratitude to Dr Ihsan ul Haq, Chairman, Department of Pharmacy, Faculty of Biological Sciences, Quaid-i-Azam University, Islamabad. We are also thankful to Prof. Dr Arif Ullah Khan for providing us with access to the MDR laboratory of Riphah International University's Riphah Institute of Pharmaceutical Sciences, which facilitated our work.

References

1 N. A. Elkanzi, H. Hrichi, R. A. Alolayan, W. Derafa, F. M. Zahou and R. B. Bakr, Synthesis of chalcones derivatives and their biological activities: a Review, *ACS Omega*, 2022, **7**, 27769–27786.
2 I. Erdem, S. Aktas and S. Ogut, Neohesperidin dihydrochalcone ameliorates experimental colitis *via* anti-inflammatory, antioxidative, and antiapoptosis effects, *J. Agric. Food Chem.*, 2024, **72**, 15715–15724.
3 R. Arif, M. Rana, S. Yasmeen, M. S. Khan, M. Abid and M. Khan, Facile synthesis of chalcone derivatives as antibacterial agents: Synthesis, DNA binding, molecular docking, DFT and antioxidant studies, *J. Mol. Struct.*, 2020, **1208**, 127905.
4 P. Thapa, S. P. Upadhyay, W. Z. Suo, V. Singh, P. Gurung, E. S. Lee, R. Sharma and M. Sharma, Chalcone and its analogs: Therapeutic and diagnostic applications in Alzheimer's disease, *Bioorg. Chem.*, 2021, **108**, 104681.
5 N. S. Ibrahim, H. A. Sayed, M. Sharaky, H. M. Diab, A. H. Elwahy and I. A. Abdelhamid, Synthesis, cytotoxicity, anti-inflammatory, anti-metastatic and anti-oxidant activities of novel chalcones incorporating 2-phenoxy-N-arylacetamide and thiophene moieties: induction of

apoptosis in MCF7 and HEP2 cells, *Naunyn-Schmiedeberg's Arch. Pharmacol.*, 2024, 1–17.
6 M. Akimoto, R. Maruyama, Y. Kawabata, Y. Tajima and K. Takenaga, Antidiabetic adiponectin receptor agonist AdipoRon suppresses tumour growth of pancreatic cancer by inducing RIPK1/ERK-dependent necroptosis, *Cell Death Dis.*, 2018, **9**, 804.
7 A. S. Yekkirala, D. P. Roberson, B. P. Bean and C. J. Woolf, Breaking barriers to novel analgesic drug development, *Nat. Rev. Drug Discovery*, 2017, **16**, 545–564.
8 P. V. Abbott, Present status and future directions: managing endodontic emergencies, *Int. Endod. J.*, 2022, **55**, 778–803.
9 K. Y. Ho, M. S. Cardosa, S. Chaiamnuay, R. Hidayat, H. Q. T. Ho, O. Kamil, S. A. Mokhtar, K. Nakata, S. V. Navarra and V. H. Nguyen, Practice advisory on the appropriate use of NSAIDs in primary care, *J. Pain Res.*, 2020, **13**, 1925–1939.
10 H. Suleyman, B. Demircan and Y. Karagoz, Anti-inflammatory and side effects of cyclo-oxygenase inhibitors, *Pharmacol. Rep.*, 2007, **59**, 247.
11 O. Alshazly, G. E. D. A. Abuo Rahma, M. F. Mohamed and M. Abdel Aziz, Amide linked chalcone derivatives, a promising class of compounds with versatile biological effects, *RSC Adv.*, 2025, **15**, 19043–19068.
12 S. Kumari, A. V. Carmona, A. K. Tiwari and P. C. Trippier, Amide bond bioisosteres: Strategies, synthesis, and successes, *J. Med. Chem.*, 2020, **63**, 12290–12358.
13 N. A. Meanwell, Applications of bioisosteres in the design of biologically active compounds, *J. Agric. Food Chem.*, 2023, **71**, 18087–18122.
14 M. F. Elahi, G. Guan and L. Wang, Hemocompatibility of surface modified silk fibroin materials: A review, *Rev. Adv. Mater. Sci.*, 2014, **38**, 148–159.
15 T. H. Do, D. M. Nguyen, V. D. Truong, T. H. T. Do, M. T. Le, T. Q. Pham, K. M. Thai and T. D. Tran, Synthesis and selective cytotoxic activities on rhabdomyosarcoma and noncancerous cells of some heterocyclic chalcones, *Molecules*, 2016, **21**, 329.
16 Y. Ouyang, J. Li, X. Chen, X. Fu, S. Sun and Q. Wu, Chalcone derivatives: Role in anticancer therapy, *Biomolecules*, 2021, **11**, 894.
17 L. F. B. Bortolotto, B. C. Azevedo, G. Silva, M. Marins and A. L. Fachin, Cytotoxic activity evaluation of chalcones on human and mouse cell lines, *BMC Proc.*, 2014, **8**, P52.
18 H. O. Saxena, U. Faridi, J. K. Kumar, S. Luqman, M. P. Darokar, K. Shanker, C. S. Chanotiya, M. M. Gupta and A. S. Negi, Synthesis of chalcone derivatives on steroidal framework and their anticancer activities, *Steroids*, 2007, **72**, 892–900.
19 F. de Campos Buzzi, P. Padaratz, A. V. Meira, R. Corrêa, R. J. Nunes and V. Cechinel Filho, 4-Acetamidochalcone derivatives as potential antinociceptive agents, *Molecules*, 2007, **12**, 896–906.
20 A. Razmi, A. Zarghi, S. Arfaee, N. Naderi and M. Faizi, Evaluation of antinociceptive and anti-inflammatory activities of novel chalcone derivatives, *Iran. J. Pharm. Res.*, 2013, **12**, 153.
21 D. Naidoo, A. Roy, L. P. Slavětínská, J. Chukwujekwu, S. Gupta and J. Van Staden, New role for crinamine as a potent, safe and selective inhibitor of human monoamine oxidase B: *In vitro* and *in silico* pharmacology and modeling, *J. Ethnopharmacol.*, 2020, **248**, 112305.
22 S. Udugade, R. Doijad and B. Udugade, In silico evaluation of pharmacokinetics, drug-likeness and medicinal chemistry friendliness of momordicin1: An active chemical constituent of Momordica charantia, *J. Adv. Sci. Res.*, 2019, **10**, 222–229.
23 A. Daina, O. Michielin and V. Zoete, SwissADME: a free web tool to evaluate pharmacokinetics, drug-likeness and medicinal chemistry friendliness of small molecules, *Sci. Rep.*, 2017, **7**, 42717.
24 M. Aarjane, A. Aouidate, S. Slassi and A. Amine, Synthesis, antibacterial evaluation, *in silico* ADMET and molecular docking studies of new N-acylhydrazone derivatives from acridone, *Arab. J. Chem.*, 2020, **13**, 6236–6245.
25 D. Baker, A surprising simplicity to protein folding, *Nature*, 2000, **405**, 39–42.
26 R. R. Ji, A. Chamessian and Y. Q. Zhang, Pain regulation by non-neuronal cells and inflammation, *Science*, 2016, **354**, 572–577.
27 J. R. Vane and R. M. Botting, Mechanism of action of anti-inflammatory drugs, *Adv. Prostaglandin Thromboxane Leukotriene Res.*, 1997, **23**, 131–138.
28 M. A. Bhat, M. A. Al Omar, M. Raish, M. A. Ansari, H. A. Abuelizz, A. H. Bakheit and A. M. Naglah, Indole derivatives as cyclooxygenase inhibitors: synthesis, biological evaluation and docking studies, *Molecules*, 2018, **23**, 1250.
29 J. R. Deuis, L. S. Dvorakova and I. Vetter, Methods used to evaluate pain behaviors in rodents, *Front. Mol. Neurosci.*, 2017, **10**, 284.
30 C. Giglio, H. L. A. Defino, C. Da Silva, A. De Souza and E. A. Del Bel, Behavioral and physiological methods for early quantitative assessment of spinal cord injury and prognosis in rats, *Braz. J. Med. Biol. Res.*, 2006, **39**, 1613–1623.
31 S. Irwin, D. R. Bennett, L. C. Hendershot, M. Seevers and R. W. Houde, The effects of morphine, methadone and meperidine on some reflex responses of spinal animals to nociceptive stimulation, *J. Pharmacol. Exp. Ther.*, 1951, **101**, 132–143.
32 R. Koster, M. Anderson and E. J. De Beer, Acetic acid for analgesic screening, *Fed. Proc.*, 1959, **18**, 412–417.
33 F. F. Rodrigues, *et al.*, Synthesis and antinociceptive evaluation of chalcone derivatives in mice, *Eur. J. Med. Chem.*, 2013, **63**, 214–223.
34 R. Corrêa, B. P. Fenner, F. de C. Buzzi, V. C. Filho and R. J. Nunes, Antinociceptive activity and preliminary structure-activity relationship of chalcone-like compounds, *Z. Naturforsch., C:J. Biosci.*, 2008, **63**, 830–836.
35 A. Razmi, A. Zarghi, S. Arfaee, N. Naderi and M. Faizi, Evaluation of anti-nociceptive and anti-inflammatory activities of novel chalcone derivatives, *Iran. J. Pharm. Res.*, 2013, **12**, 153.

36 S. Mehrzadi, H. Khalili, I. Fatemi, A. Malayeri, A. Siahpoosh and M. Goudarzi, Zingerone mitigates carrageenan-induced inflammation through antioxidant and anti-inflammatory activities, *Inflammation*, 2021, **44**, 186–193.

37 Z. Ou, J. Zhao, L. Zhu, L. Huang, Y. Ma, C. Ma, C. Luo, Z. Zhu, Z. Yuan and J. Wu, Anti-inflammatory effect and potential mechanism of betulinic acid on λ-carrageenan-induced paw edema in mice, *Biomed. Pharmacother.*, 2019, **118**, 109347.

38 H. S. Semis, C. Gur, M. Ileriturk, O. Kaynar and F. M. Kandemir, Investigation of the anti-inflammatory effects of caffeic acid phenethyl ester in a model of λ-Carrageenan-induced paw edema in rats, *Hum. Exp. Toxicol.*, 2021, **40**, S721–S738.

39 I. Jantan, S. N. A. Bukhari, O. A. Adekoya and I. Sylte, Studies of synthetic chalcone derivatives as potential inhibitors of secretory phospholipase A2, cyclooxygenases, lipoxygenase and pro-inflammatory cytokines, *Drug Des. Dev. Ther.*, 2014, **8**, 1405–1418.

40 D. K. Mahapatra, S. K. Bharti and V. Asati, Chalcone derivatives: anti-inflammatory potential and molecular targets perspectives, *Curr. Top. Med. Chem.*, 2017, **17**, 3146–3169.

41 D. K. Mahapatra, V. Asati and S. K. Bharti, Perspectives of chalcone-based NF-κB inhibitors as anti-inflammatory agents, in *Biologically Active Small Molecules*, Apple Academic Press: Palm Bay, FL, 2023, pp. 45–58.

42 K. Liaras, M. Fesatidou and A. Geronikaki, Thiazoles and thiazolidinones as COX/LOX inhibitors, *Molecules*, 2018, **23**, 685.

43 T. Martins, B. M. Fonseca and I. Rebelo, Antioxidant effects of chalcones during the inflammatory response: an overall review, *Curr. Med. Chem.*, 2021, **28**, 7658–7713.

44 Y. Ouyang, J. Li, X. Chen, X. Fu, S. Sun and Q. Wu, Chalcone derivatives: role in anticancer therapy, *Biomolecules*, 2021, **11**, 894.

45 H. R. Choi, H. Lim, J. H. Lee, H. Park and H. P. Kim, Interruption of Helicobacter pylori-induced NLRP3 inflammasome activation by chalcone derivatives, *Biol. Ther.*, 2021, **29**, 410.

46 V. R. Yadav, S. Prasad, B. Sung and B. B. Aggarwal, The role of chalcones in suppression of NF-κB-mediated inflammation and cancer, *Int. Immunopharmacol.*, 2011, **11**, 295–309.

47 M. L. Liu, Y. H. Duan, Y. L. Hou, C. Li, H. Gao, Y. Dai and X. S. Yao, Nardoaristolones A and B, two terpenoids with unusual skeletons from Nardostachys chinensis Batal, *Org. Lett.*, 2013, **15**, 1000–1003.

48 A. J. Bussmann, T. H. Zaninelli, T. Saraiva-Santos, V. Fattori, C. F. Guazelli, M. M. Bertozzi, K. C. Andrade, C. R. Ferraz, D. Camilios-Neto, A. M. Casella and R. Casagrande, The flavonoid hesperidin methyl chalcone targets cytokines and oxidative stress to reduce diclofenac-induced acute renal injury: Contribution of the Nrf2 redox-sensitive pathway, *Antioxidants*, 2022, **11**, 1261.

49 V. Kotra, S. Ganapaty and S. R. Adapa, Synthesis of a new series of quinolinyl chalcones as anticancer and anti-inflammatory agents, *Indian J. Chem., Sect. B*, 2010, **49**, 1109–1116.

50 H. Rücker, N. Al Rifai, A. Rascle, E. Gottfried, L. Brodziak-Jarosz, C. Gerhäuser, T. P. Dick and S. Amslinger, Enhancing the anti-inflammatory activity of chalcones by tuning the Michael acceptor site, *Org. Biomol. Chem.*, 2015, **13**, 3040–3047.

51 L. Zheng, Y. Li, D. Wu, H. Xiao, S. Zheng, G. Wang and Q. Sun, Development of covalent inhibitors: Principle, design, and application in cancer, *MedComm: Oncol.*, 2023, **2**, e56.

52 A. F. Yepes, J. Quintero-Saumeth and W. Cardona-G, Chalcone-quinoline conjugates as potential T. cruzi cruzipain inhibitors: docking studies, molecular dynamics and evaluation of drug-likeness, *ChemistrySelect*, 2020, **5**, 7104–7112.

53 Y. Luo, Z. Yang, Y. Zhang, S. Jiang, J. Zhu, X. Li, Q. You and M. Lu, Patenting perspective on Keap1 inhibitors (2019–2024), *Expert Opin. Ther. Pat.*, 2025, **35**, 325–356.

54 M. Berredjem, F. Bouchareb, S. E. Djouad, R. Bouasla, R. Bahadi, R. Redjemia, M. Boussaker and A. Dekir, Recent progress in synthesis of sulfonamides and N-acylsulfonamides, biological applications and their structure-activity relationship (SAR) studies, *ChemistrySelect*, 2023, **8**, e202301859.

55 M. Al-Mamary, S. A. Al-Mikhlafi and B. Jaadan, Synthesis and biological activities of some chalcone derivatives, *Int. J. Chem. Pharm. Sci.*, 2014, **5**, 61–68.

56 S. Katke, S. Amrutkar, R. Bhor and M. Khairnar, Synthesis of biologically active 2-chloro-N-alkyl/aryl acetamide derivatives, *Int. J. Pharma Sci. Res.*, 2011, **2**, 148–156.

57 E. Abdel-Latif, M. M. Fahad and M. A. Ismail, Synthesis of N-aryl 2-chloroacetamides and their chemical reactivity towards various types of nucleophiles, *Synth. Commun.*, 2020, **50**, 289–314.

58 A. Zafar, Y. Wasti, M. Majid, D. Muntaqua, S. G. Bungau and I. U. Haq, Artemisia brevifolia Wall. ex DC enhances cefixime susceptibility by reforming antimicrobial resistance, *Antibiotics*, 2023, **12**, 1553.

59 S. S. Zahra, M. Ahmed, M. Qasim, B. Gul, M. Zia, B. Mirza and I. U. Haq, Polarity-based characterization of biologically active extracts of Ajuga bracteosa Wall. ex Benth. and RP-HPLC analysis, *BMC Complementary Altern. Med.*, 2017, **17**, 1.

60 T. Mosmann, Rapid colorimetric assay for cellular growth and survival: Application to proliferation and cytotoxicity assays, *J. Immunol. Methods*, 1983, **65**, 55–63.

61 S. M. Masaud, H. Nadeem and A. Shamim, Discovery of a novel orally active ketamine derivative with dual analgesic and antidepressant activities, lacking psychomimetic effects, *ACS Chem. Neurosci.*, 2025, **16**, 932–944.

62 S. M. Masaud, H. Nadeem, A. Shamim, M. K. Zargaham, U. Shareef, S. Ayaz and B. M. Murtaza, Synthesis, biological evaluation, and *in silico* studies of chalcone-based ketamine derivatives with preferential COX-2 inhibitory activity, *Med. Chem. Res.*, 2025, **34**, 1779–1805.

63 O. M. Alshehri, A. Zeb, S. M. Mukarram Shah, M. H. Mahnashi, S. A. Asiri, O. Alqahtani, A. Sadiq, M. Ibrar, S. Alshamrani and M. S. Jan, Investigation of anti-nociceptive, anti-inflammatory potential and ADMET studies of pure compounds isolated from Isodon rugosus Wall. ex Benth, *Front. Pharmacol*, 2024, **15**, 1328128.

64 M. Ahmadi, S. Bekeschus, K. D. Weltmann, T. von Woedtke and K. Wende, Non-steroidal anti-inflammatory drugs: Recent advances in the use of synthetic COX-2 inhibitors, *RSC Med. Chem.*, 2022, **13**, 471–496.

65 H. Guterres and W. Im, Improving protein-ligand docking results with high-throughput molecular dynamics simulations, *J. Chem. Inf. Model.*, 2020, **60**, 2189–2198.

66 S. Jo, T. Kim, V. G. Iyer and W. Im, CHARMM-GUI: A web-based graphical user interface for CHARMM, *J. Comput. Chem.*, 2008, **29**, 1859–1865.

67 R. B. Best, X. Zhu, J. Shim, P. E. M. Lopes, J. Mittal, M. Feig and A. D. MacKerell Jr., Optimization of the additive CHARMM all-atom protein force field targeting improved sampling of the backbone φ, ψ, and side-chain χ1 and χ2 dihedral angles, *J. Chem. Theory Comput.*, 2012, **8**, 3257–3273.

68 J. Huang and A. D. MacKerell Jr., CHARMM36 all-atom additive protein force field: validation based on comparison to NMR data, *J. Comput. Chem.*, 2013, **34**, 2135–2145.

69 K. Vanommeslaeghe, E. Hatcher, C. Acharya, S. Kundu, S. Zhong, J. Shim, E. Darian, O. Guvench, P. Lopes, I. Vorobyov and A. D. MacKerell Jr., Automation of the CHARMM general force field (CGenFF) I: Bond perception and atom typing, *J. Comput. Chem.*, 2010, **31**, 671–690.

70 W. L. Jorgensen, J. Chandrasekhar, J. D. Madura, R. W. Impey and M. L. Klein, Comparison of simple potential functions for simulating liquid water, *J. Chem. Phys.*, 1983, **79**, 926–935.

71 M. J. Abraham, T. Murtola, R. Schulz, S. Páll, J. C. Smith, B. Hess and E. Lindahl, GROMACS: High performance molecular simulations through multi-level parallelism from laptops to supercomputers, *SoftwareX*, 2015, **1–2**, 19–25.

72 M. Parrinello and A. Rahman, Polymorphic transitions in single crystals: A new molecular dynamics method, *J. Appl. Phys.*, 1981, **52**, 7182–7190.

73 G. Bussi, D. Donadio and M. Parrinello, Canonical sampling through velocity rescaling, *J. Chem. Phys.*, 2007, **126**, 014101.

74 J. Higgs, C. Wasowski, A. Marcos, M. Jukič, C. H. Paván, S. Gobec, F. de Tezanos Pinto, N. Colettis and M. Marder, Chalcone derivatives: synthesis, *in vitro* and *in vivo* evaluation of their anti-anxiety, anti-depression and analgesic effects, *Heliyon*, 2019, **5**, e01376.

75 G. Viana, M. Bandeira and F. Matos, Analgesic and anti-inflammatory effects of chalcones isolated from *Myracrodruon urundeuva* Allemão, *Phytomedicine*, 2003, **10**, 189–195.

76 R. Koster, W. Anderson and E. De Beer, Acetic acid for analgesic screening, *Fed. Proc.*, 1959, **18**, 412–417.

77 S. P. Gawade, Acetic acid-induced painful endogenous infliction in writhing test on mice, *J. Pharmacol. Pharmacother.*, 2012, **3**, 348.

78 N. A. A. Bakar, M. R. Sulaiman, N. Lajis, M. N. Akhtar and A. S. Mohamad, Evaluation of antinociceptive profile of chalcone derivative (3-(2,5-dimethoxyphenyl)-1-(5-methylfuran-2-yl)prop-2-en-1-one) (DMPF-1) in vivo, *J. Pharm. BioAllied Sci.*, 2020, **12**, S711–S717.

79 C. A. Winter, E. A. Risley and G. W. Nuss, Carrageenin-induced edema in hind paw of the rat as an assay for anti-inflammatory drugs, *Proc. Soc. Exp. Biol. Med.*, 1962, **111**, 544–547.

80 R. M. E. Al-Nuaimy and N. S. Al-Azzo, Evaluation of the expression of immunohistochemical staining of PDL1 in renal cell cancer, *Iraqi J. Pharm. Sci.*, 2024, **21**, 9–14.

81 I. Malik, F. A. Shah, T. Ali, Z. Tan, A. Alattar, N. Ullah, A.-U. Khan, R. Alshaman and S. Li, Potent natural antioxidant carveol attenuates MCAO-stress induced oxidative, neurodegeneration by regulating the Nrf-2 pathway, *Front. Neurosci.*, 2020, **14**, 659.

82 World Health Organization, *WHO guidelines on drawing blood: Best practices in phlebotomy*, World Health Organization, Geneva, 2010. https://www.who.int/publications/i/item/9789241599221.